

ABSTRACT

VIABILITY OF CERIUM OXIDE NANOPARTICLES AS A RADIOPROTECTOR AGAINST PROTON RADIATION FOR NON-MALIGNANT CELLS

by Brian W. Swartz

May 2015

Director of Dissertation: Jefferson Shinpaugh, PhD.

DEPARTMENT OF PHYSICS

Radiation therapy is a prevalent cancer treatment therapy. The goal is to kill all tumor cells while minimizing damage to healthy cells and new methods that can accomplish this goal are continually being investigated. Cerium Oxide (CeO_2) or ceria nanoparticles have recently shown to act as a radioprotector for non-malignant cells while sensitizing tumor cells to x-rays. However, research is required to determine if the same benefits are present for heavy charged-particle radiation. This dissertation research investigates the efficacy of ceria nanoparticles (CNPs) as a radioprotector of normal cells irradiated with 3-4 MeV protons at doses of 1-6 Gy in the East Carolina University Accelerator Laboratory. The CNPs were synthesized at the University of Central Florida Nanoscience Technology Center and were transferred to ECU. Cell viability was measured with the Microculture Tetrazolium (MTT) assay 24 and 48 hours post irradiation. DNA damage was determined using the Terminal Uridine Nick-End Labeling (TUNEL) assay. While showing promise for potential radioprotection of non-malignant cells using both assays, the MTT assay results were less conclusive and require further research. The TUNEL assay results are preliminary but show that CNPs reduce DNA damage to non-malignant cells compared to those cells which were not treated.

**VIABILITY OF CERIUM OXIDE NANOPARTICLES AS A RADIOPROTECTOR
AGAINST PROTON RADIATION FOR NON-MALIGNANT CELLS**

A Dissertation

Presented To

The Faculty of the Department of Physics

East Carolina University

In Partial Fulfillment of the Requirements for the Degree Doctor of Philosophy in Biomedical
Physics

by

Brian W. Swartz

May 2015

© Brian W. Swartz, 2015

VIABILITY OF CERIUM OXIDE NANOPARTICLES AS A RADIOPROTECTOR AGAINST
PROTON RADIATION FOR NON-MALIGNANT CELLS

By

Brian W. Swartz

APPROVED BY:

DISSERTATION ADVISOR _____
Jefferson Shinpaugh, Ph.D.

COMMITTEE MEMBER _____
Roberta M. Johnke, Ph.D.

COMMITTEE MEMBER _____
Michael Dingfelder, Ph.D.

COMMITTEE MEMBER _____
Cindy Putnam-Evans, Ph.D.

COMMITTEE MEMBER _____
John Kenney, Ph.D.

COMMITTEE MEMBER _____
Ziwei Lin, Ph.D.

CHAIR OF THE DEPARTMENT OF PHYSICS _____
John C. Sutherland, Ph.D.

DEAN OF THE GRADUATE SCHOOL _____
Paul J. Gemperline, Ph.D.

DEDICATION

This work is dedicated to my wife, Leah.

ACKNOWLEDGEMENTS

I would like to thank my advisor Dr. Jeff Shinpaugh for being a great mentor and advisor on not only my academics but life in general. He showed constant support and encouragement as we toiled through the renovation and installation of the new accelerator and gave a great example of how a research scientist and professor should be. I have to thank the ECU Accelerator support group: Chris, Gene, William and Mike for helping me with both the little and big things to help this dissertation come to fruition. I would also like to thank Dr. Cindy Putnam-Evans and Jianfen Lu for all the help and patience in helping a physicist learn the world of cell biology. Also, I have to thank the members of my committee: Dr. Roberta Johnke, Dr. Michael Dingfelder, Dr. Ziwei Lin and Dr. John Kenney for all their feedback and advice in completing this dissertation.

My wife deserves all my gratitude for her patience as I worked toward my goals and giving me love and support for the whole journey. My parents, Bruce and Valerie Swartz, and sister Stephanie have stood behind me and offered many prayers for me to help me find and grow my love of science. Most importantly, I give thanks to my heavenly Father for giving me the grace and wisdom to accomplish my dream.

Table of Contents

| | |
|---|----|
| LIST OF FIGURES..... | ix |
| LIST OF ABBREVIATIONS..... | xi |
| Chapter 1: Introduction..... | 1 |
| Photons..... | 2 |
| Neutrons..... | 3 |
| Electrons..... | 4 |
| Protons and Charged Ions..... | 5 |
| Radiation Damage and Protection..... | 6 |
| Chapter 2: Radiation Dose Theory and Radiation Biology..... | 8 |
| Stopping Power..... | 8 |
| Restricted Stopping Power and LET..... | 9 |
| Energy and Range Straggling..... | 10 |
| Dose Measurements for Charged Particles..... | 10 |
| Dose Calculations for Charged Particle Beams..... | 11 |
| 2.2 Biological and Chemical effects of Radiation..... | 12 |
| Chemical and physical changes in irradiated water..... | 12 |
| Biological Effects of Radiation..... | 13 |
| 2.3 Radioprotectors..... | 15 |

| | |
|--|----|
| Amifostine and other Synthetic Radioprotectors | 15 |
| Natural Radioprotectors | 17 |
| Cerium Oxide Nanoparticles..... | 19 |
| 2.4 Hypothesis and Specific Aims | 23 |
| Specific Aim 1 | 23 |
| Specific Aim 2 | 24 |
| Specific Aim 3 | 24 |
| Chapter 3: Materials and methods | 25 |
| 3.1 Research Design..... | 25 |
| Accelerator System and External Beamline at ECU..... | 25 |
| Beam Dose Calculation and Profiling..... | 30 |
| Cell lines and Culture Conditions | 33 |
| CNP and WR-1065 Preparation..... | 35 |
| Cell Survival and DNA damage assay | 37 |
| 3.2 Research Experiment Methods | 37 |
| 3.3 MTT and TUNEL Assays..... | 38 |
| Chapter 4: Results | 42 |
| 4.1 Dose Adjustments | 42 |
| 4.2 CNP survival results with 3 MeV protons | 43 |

| | |
|--|----|
| 1 Gy Proton Dose Results | 44 |
| 3 Gy Results | 46 |
| 4 Gy Results | 49 |
| 4.3 Survival Curve of 3 MeV and 4 MeV Proton Irradiation | 50 |
| 4.4 4 MeV Proton Irradiation Data | 54 |
| 4.5 TUNEL Assay Data | 59 |
| Chapter 5: Discussion | 62 |
| 5.1 Radiation Beam Dose Measurement System | 62 |
| 5.2 Cell Survival Data..... | 63 |
| 5.3 DNA Damage Assay..... | 66 |
| 5.4 Future Directions | 66 |
| References..... | 68 |

LIST OF FIGURES

| | |
|--|----|
| Figure 3.1 ECU Particle Accelerator layout..... | 26 |
| Fig. 3.2 15° beamline side view of irradiation setup..... | 28 |
| Fig. 3.3 End of beamline setup..... | 30 |
| Fig. 3.4 Sample Beam Intensity Image..... | 33 |
| Fig. 4.1 YAG crystal image of beam profile including scatter..... | 43 |
| Fig. 4.2 Surviving fraction of CNP treated cells at 1.1 Gy (3 MeV)..... | 44 |
| Fig. 4.3 Surviving fraction of CNP treated cells at 1.1 Gy (3 MeV)..... | 45 |
| Fig. 4.4 Surviving fraction of CNP treated cells at 1.1 Gy (3 MeV)..... | 46 |
| Fig. 4.5 Surviving fraction of CNP treated cells at 3.6 Gy (3 MeV) | 47 |
| Fig. 4.6 Surviving fraction of CNP treated cells at 4.4 Gy (3 MeV)..... | 49 |
| Fig. 4.7 Linear quadratic fit of cell survival curve for 4 MeV protons | 50 |
| Fig. 4.8 Survival Curve fitted with Linear Quadratic model..... | 52 |
| Fig. 4.9 Cell Survival curve from 3 MeV proton radiation | 53 |
| Fig. 4.10a and b. Surviving fraction of CNP treated cells at 1 Gy (4 MeV)..... | 54 |

| | |
|--|----|
| Fig. 4.11 Surviving fraction of CNP treated cells at 1 Gy (4 MeV)..... | 55 |
| Fig. 4.12 Time of application of the CNPs to the cells..... | 56 |
| Fig. 4.13 24 vs. 48 hour assay..... | 58 |
| Fig. 4.14. TUNEL images showing DNA damage (red) and DNA (blue)..... | 60 |
| Fig. 4.15 TUNEL images merged with both the DAPI and the TUNEL..... | 61 |

LIST OF ABBREVIATIONS

| | |
|-------|--|
| ACR | Acute Radiation Syndrome |
| AOT | Sodium bis(2-ethylhexyl) sulfosuccinate |
| BSA | Bovine serum albumin |
| CNP | Cerium oxide nanoparticle |
| DAPI | 4',6-DiAmidino-2-phenylindole |
| DNA | Deoxyribonucleic acid |
| DRF | Dose reduction factor |
| dUTP | Deoxyuridine triphosphate |
| ECU | East Carolina University |
| EDTA | Ethylenediaminetetraacetic acid |
| EdUTP | Ethynyl- deoxyuridine triphosphate |
| FDA | Food and Drug Administration |
| F.C. | Faraday Cup |
| GI | Gastrointestinal |
| Gy | Gray |
| HRTEM | High-resolution transmission electron microscopy |

| | |
|----------|---|
| IL-1 | Interleukin-1 |
| LD 50/30 | Lethal dose to 50% of the population in 30 days |
| LET | Linear Energy Transfer |
| MEBM | Mammal epithelial basal medium |
| MTT | Methylthiazol tetrazolium |
| MV | Megavolts |
| NEC | National Electrostatics Corporation |
| NSTC | Nanoscience and Technology Center |
| OTC | Over the counter |
| PBS | Phosphate-buffered saline |
| RMS | Root mean square |
| RNA | Ribonucleic acid |
| ROS | Reactive oxygen species |
| SOD | Superoxide dismutase |
| SRIM | Stopping powers and ranges of ions in matter |
| TdT | Terminal deoxynucleotidyl transferase |

TUNEL Terminal Uridine Nick-End Labeling

UCF University of Central Florida

YAG Yttrium aluminum garnet

Chapter 1: Introduction

Ionizing radiation impacts humanity in many areas of daily life from occupational hazards to medical applications. Between 1982 and 2006, the radiation exposure per capita increased 600% from medical exposure alone.[1] The average American receives a radiation dose of about 620 millirem each year, half it coming from background radiation.[2] It can be advantageous in areas of medicine, research, agriculture and energy, but it can also be a danger to people as well. One particular area of concern is the exposure of people to radiation from uncontrolled sources in cases of industrial accidents, terrorism, and space travel.[3, 4] Excess exposure can cause immediate effects such as radiation sickness as well as long term effects such as cancer.[5] In regards to long term space travel, adequate medical care may not be available for astronauts suffering from short term effects, so ongoing research is being conducted to find methods of prevention and mitigation of radiation effects.[6]

As radiation travels through matter, it interacts with orbital electrons and the atomic nuclei by either elastic, inelastic or absorption events. The kinetic energy can be deposited along the path of the radiation with the amount and distribution being dependent upon the type of radiation and the interactions taking place between the particles within the matter and the radiation. This deposited energy can cause excitation or ionization of atoms within the target, allowing it to absorb the energy and thereby reducing the intensity of the incident radiation. When the atoms are ionized, the electrons overcome their binding energy, carrying energy that can either be deposited locally or farther away from their original location. The measurement of this energy deposition in matter is defined as dose, measured in Gray (Gy).[5]

The deposition of dose can be facilitated by several different forms of radiation, both particulate and electromagnetic. Each form has several methods of interaction in matter and several ways of depositing energy within that matter. Photons and x-rays are considered electromagnetic radiation and protons, neutrons, electrons and heavy ions are considered particulate radiation and are discussed in further detail here.

Photons

Coherent scattering – Coherent scattering, also known as Rayleigh scattering, takes place when photons interact elastically with the atom and do not transfer energy to the atom. This interaction type dominates at photon energies below 10 keV.

Photoelectric Effect- Photoelectric effect takes place when the incident photon is absorbed completely by the target atom causing ionization which results in an inner shell electron being ejected from the atom. The vacancy left behind leaves the atom in an excited state which causes a de-excitation process involving an outer electron falling to the inner orbit to fill the vacancy. This transition results in the emission of secondary radiation in the form of characteristic X-rays and/or Auger electrons. The probability of the photoelectric effect is inversely proportional to the photon energy, dominating at energies up to 500 keV; and directly proportional to the atomic number Z , dominating at $Z > 20$. [7]

Compton Effect – As the energy of the incident photon increases, some of the energy is deposited in the atom when the photon and the orbital electron interact and the electron recoils to conserve momentum. In this case, the incident photon energy is much greater than the orbital electron energy so as a result of the collision, the electron is ejected from the atom while the photon is scattered to undergo further interactions, losing more energy until the photon is finally absorbed

by an orbital electron. The Compton electron also undergoes interactions until an atom captures it. The subsequent events of Compton scattering are the source of dose deposition within the target which will be discussed in greater detail later. The probability of Compton scattering is nearly independent of the atomic number of the target atoms and primarily is inversely proportional to the photon energy. The Compton effect dominates over a wide range of energies between 100 keV to 10 MeV. [7]

Pair Production- When the incident photon reaches the threshold energy of 1.022 MeV, it is possible for it to interact with a nuclear field and annihilate resulting in the creation of an electron-positron pair. The threshold energy represents the total rest mass of the pair while any excess energy over the threshold is shared as kinetic energy between the electron-positron pair. The probability of pair production increases with increasing atomic number as well as increasing photon energy above the threshold energy. The electron encounters subsequent interactions within the target while the positron interacts with an electron and annihilates, creating two 511-keV photons emitted in opposite directions. This photon creation allows for the conservation of momentum and energy. Just as in the Compton Effect interaction, the subsequent electrons and photons interact throughout the target material, depositing their energy.

Neutrons

Neutrons primarily interact with atomic nuclei through either elastic scattering (neutron moderation) or inelastic scattering (neutron resonance scattering). Absorption can also take place in the form of a nuclear reaction. Due to the small cross section of neutrons and their neutral charge, they have no definitive range of penetration.[8] Neutrons are more likely to transfer

energy to atomic nuclei, specifically those that are light in mass, such as hydrogen nuclei (single protons) which have almost the same mass as the neutron and recoil in the interaction taking a significant amount of the neutron's kinetic energy. Heavy atomic nuclei ($Z > 20$) only receive a small fraction of the neutron's energy in the interaction which contributes to a long range for the neutron.[9] Fast moving neutrons ($0.1 \text{ MeV} < E < 10 \text{ MeV}$) tend to interact through elastic collisions while slow or thermal neutrons tend to be captured by nuclei to form radioactive isotopes.[9] The mechanism of dose deposition in the target is the result of the recoil protons interacting within the target medium.

Electrons

The Coulomb force governs the interaction of electrons in matter with the primary interaction taking place between the incoming electrons and the orbital electrons. When the electrons interact elastically, it is referred to as Rutherford scattering. Inelastic events with the atomic nuclei can result in bremsstrahlung radiation or "braking" radiation where the electron emits a photon as it interacts with a nuclear field. Bremsstrahlung radiation can occur when electrons experience deceleration from the interaction with another charged particle, usually the atomic nucleus. This can cause a change in kinetic energy which produces a photon with the same energy. These bremsstrahlung photons can then interact in all the ways described previously in the last section. Bremsstrahlung contamination when determining dose makes up less than 1% at 4 MeV electrons and less than 4% for 20 MeV electrons.[10] Since the masses are the same for the incoming electron and the orbital electron, large energy losses and wide scattering angles are common resulting in tortuous paths within the target material. Their penetration paths are short compared to photon paths and the energy loss is continuous over the range of the electron as opposed to the energy loss of photons. As the electron slows down towards the end of its range,

the deposition of energy increases due to the strong dependence of the ionization cross section on the velocity but due to their small mass, the deposition of energy is widespread within the target. For low Z targets ($Z < 10$), the electrons primarily interact with the orbital electrons resulting in loss of energy due to ionization.[11] If the energy is sufficient, secondary electrons, also called delta rays, can result from further ionization.[9] For low z targets, the occurrence of bremsstrahlung is a rare occurrence since it is a function of Z^2 of the target.

Protons and Charged Ions

Similar to electrons, heavy charged particles are governed by the Coulomb force and involve Rutherford scattering. Similar to neutrons, they can undergo the absorption process into an atomic nuclei. The principle method by which heavy charged particles lose their energy is through ionization and excitation of orbital electrons, a process called collisional energy loss. Secondary electrons (delta rays) produced in the collisions are able to cause subsequent ionization in the target matter with sufficient energy. The rate of energy loss by the heavy charged particles is proportional to the electron density of the medium.

The probability of losing energy through bremsstrahlung radiation, also called radiative loss, increases directly with the energy of the incoming charged particle. The probability of production of bremsstrahlung by heavy charged particles is negligible at low energies with the primary energy loss mechanism taking place through ionization of target atoms. Because of their heavy mass, heavy charged particles have essentially a straight path through the target medium and tend to have a much shorter path than electrons or uncharged particles. As the heavy charged particles move through the matter, they begin to lose energy at a higher rate towards the end of their path reaching a maximum called the Bragg peak.[8] When plotting stopping power vs.

range in matter, the Bragg peak represents the point where the rate of energy loss is at a maximum. The peak is seen at greater ranges as the energy of the incident particles increases.

Radiation Damage and Protection

When charged particles and neutrons interact with DNA to cause strand breaks it is referred to as direct damage and is associated with high linear energy transfer (LET) radiation.[12] Direct damage tends to be more damaging, causing more DNA double-strand breaks which are more difficult for the cell to repair. Low LET radiation causes molecules in water to ionize and creates free radicals, that cause damage to DNA strands through single strand breaks which are easier for the cell to repair.[13] Radioprotectors can improve cell survival by removing free radicals by providing valence electrons that bind to the radicals and neutralize them. A more detailed description is provided in the literature.[14] The current gold standard of radioprotection, amifostine, is a Food and Drug Administration (FDA) approved radioprotector and it is widely used in radiation therapy procedures to protect healthy tissues. [4] Amifostine has been shown to selectively protect a broad range of normal tissues including oral mucosa, salivary glands, lungs, bone marrow, heart, intestines, and kidneys as well as protect against cytotoxic effects of chemotherapeutic agents.[15] When biological cells are exposed to radiation, free radicals are formed through ionizing reactions which then react with DNA and RNA, which can cause chromosomal aberrations and apoptotic (cell) death. [16] Amifostine is an effective free-radical scavenger that helps prevent indirect radiation damage. However, amifostine has a short half-life in serum, requires medical personnel to administer, can have side effects such as nausea or vomiting, and is unable to protect all human organ systems. [17-19] For these reasons, it would be advantageous to find alternatives that are both an effective radioprotector of normal tissues and an effective radiosensitizers of tumor tissue in radiation therapy applications. Recently,

cerium oxide (ceria) nanoparticles (CeO_2) have been tested as suitable free radical scavengers and have shown promise in increasing cell survival while having no effect on the viability of tumor cells. [17, 20] While research has been conducted using photon (x-ray) radiation, the effect of the cerium oxide nanoparticles with regards to charged particle radiation is unknown.

This research seeks to determine these effects. The research aims are threefold: 1) design and develop a system to irradiate the cells with protons, including the development of an ion beam imaging system, 2) determine a proton radiation survival curve development of non-tumorigenic cell lines, and 3) assess DNA damage analysis of the A184 cell line with and without the presence of CeO_2 nanoparticles.

Chapter 2: Radiation Dose Theory and Radiation Biology

2.1 Dose Theory

Stopping Power

Stopping power represents the average rate of energy loss of a heavy charged particle in a medium, typically measured in units of MeV cm⁻¹ or keV/μm.[9] It is a fundamental quantity in dosimetry and radiation physics. It is often designated as $-dE/dx$ with E representing energy and x (cm) representing distance and can be calculated as

$$S(E) = -dE/dx = \mu Q_{avg} = \mu \int_{Q_{min}}^{Q_{max}} QW(Q)dQ \quad (2.1)$$

with μ representing the probability per unit length that an electronic collision will occur (also known as the attenuation coefficient) measured in cm⁻¹, Q_{avg} representing the average energy loss per collision measured in eV which is equal to the integration of the single collision energy-loss spectra. This includes the $W(Q)dQ$, the probability that a given collision will result in an energy loss between Q and Q+dQ, and Q, the energy loss for each collision measured in eV. When traveling short distances in matter, the total number of interactions is small; this could cause a substantial difference in the average energy lost by the charged particle versus the probable energy lost by said particle. Stopping power can be divided by the density of the material, ρ (g/cm³), to become the mass stopping power ($-dE/\rho dx$), measured in units of MeV cm² g⁻¹. It is a useful quantity since it expresses the rate of energy loss of the charged particle per g cm⁻² of the target medium penetrated. This means that in the case of a gas, where stopping

power depends on the pressure, the mass stopping power does not since it is accounted for by the target density.

Also, the mass stopping power does not vary greatly among materials with similar atomic compositions.[9]

Restricted Stopping Power and LET

Stopping power represents the energy lost by a charged particle as it traverses through a medium; however, it is not equal to the absorbed energy in the target especially if the target is small compared to the range of the secondary electrons produced by the incident radiation. This is common in the case for biological targets, i.e. living cells that have a diameter of the order of microns or DNA strands that are 20 Å in width. [9] Delta rays with sufficient energy can easily escape from a small volume where the radiation particle originally lost energy. Restricted stopping power is a more accurate representation of the energy that is lost that is actually absorbed in the target on the microscale.[9] The restricted stopping power is defined as the linear rate of energy loss only to collisions in which the energy transfer does not exceed a specified value Δ and is written as $-(dE/dx)_\Delta$. Different values for Δ can be selected and can be used to consult tables that give mass stopping powers for energies up to a limit of Δ . Understandably, the higher the incident radiation energy, the higher the maximum energy transfer to the secondary particle in the interaction.

In the early 1950's, the concept of LET, another form of stopping power, was introduced to characterize the rate of energy transfer per unit distance along the path of the charged particle.[7] This term is synonymous with unrestricted stopping power and can be defined in the same manner with units of keV/ μm for water.

Energy and Range Straggling

As each charged particle traverses through matter, the number of collisions, amount of energy lost due to each collision and the path length all fluctuate due to the stochastic nature of the process. Therefore, with a number of identical particles, each can have a varying energy spectrum as they pass the same point within the target, causing each to have a different path length. This is referred to as energy straggling and range straggling.[7] As the energy of the incident radiation increases, the projectile velocity increases leading to a decrease in the ionization cross section. Therefore, the range of the charged particle increases. Logically, the stopping power decreases with the increase of energy since the number of interactions decreases and the chance to slow the particle down with particle collisions becomes less probable. In order to increase probability of interaction, the energy of the charged-particle radiation must decrease, the target medium density must increase, or the target volume must be made larger to increase the chance of a collision between the charged particle and an orbital electron. The mean range is defined as the absorber thickness at which the relative count rate is 0.5 on a plot of relative count rate vs. absorber thickness. The extrapolated range can be found by extending the straight portion of the curve tail down to the axis. Range straggling for protons is not significant; for a 100 MeV protons in biological tissue, the root mean square (RMS) fluctuation in range is 0.09 cm while the range is 7.57 cm, revealing a 1.2% difference. [9] According to Monte Carlo simulations by the Stopping and Range of Ions in Matter (SRIM) code, the approximate range straggling difference for 3 and 4 MeV protons is 8%.[21] The SRIM code will be discussed later in detail.

Dose Measurements for Charged Particles

Measuring dose from charged-particle beams for radiobiological experiments is often done using ionization chambers placed at different distances incident to the charged particle

beam within the target material. The dose is proportional to the beam current and for a monoenergetic beam, the depth dose curve with a maximum dose rate in the region of the Bragg peak near the end of the particle's range with the maximum LET also present at the depth in the target. When the charged particles are relatively low-energy protons (≤ 400 MeV), the energy loss is almost entirely due to collisions with orbital electrons so the dose rate will mimic the mass stopping power curve.[9] For high energy protons, the interactions begin to become more nuclear in nature and therefore change the depth dose curve relative to the mass stopping power.[9]

Dose Calculations for Charged Particle Beams

For a uniform parallel beam of monoenergetic charged particles normally incident on a tissue slab with a fluence rate $\dot{\phi}$ measured in $\text{cm}^{-2} \text{s}^{-1}$ at a given depth of x , the dose rate at that point can be determined. A thin disc shaped volume with thickness Δx is assumed along the central axis of the beam with an area A normal to the beam. The rate of energy deposition, \dot{E} in the volume could be calculated using the collisional stopping power ($-dE/dx$):

$$\dot{E} = \dot{\phi} A \left(-\frac{dE}{dx} \right) \Delta x \quad (2.2)$$

measured in MeV s^{-1} . [9] The dose rate, \dot{D} can be determined by dividing the energy deposition by the mass, $\rho A \Delta x$,

$$\dot{D} = \frac{\dot{\phi} A \left(-\frac{dE}{dx} \right) \Delta x}{\rho A \Delta x} = \dot{\phi} \left(-\frac{dE}{\rho dx} \right) \quad (2.3)$$

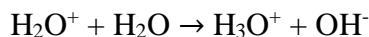
where ρ is the density of the tissue and \dot{D} is measured $\text{MeV g}^{-1} \text{s}^{-1}$. [9] Hence, the dose per unit fluence at any depth is equal to the mass stopping power for the particles at that depth, i.e., if the mass stopping power is $2 \text{ MeV cm}^2 \text{g}^{-1}$, then the dose per unit fluence can be stated as 2 MeV g^{-1}

if the fluence unit is cm^{-2} . As mentioned earlier, for high energy charged particles, the depth dose curves cannot be calculated and Monte Carlo calculations must be performed due to the substantial nuclear interactions that take place. These calculations consider each individual interaction and their cross sections and determine the outcome statistically. Due to the energies (<5 MeV) used in this research, Monte Carlo calculations were not required to determine the dose.

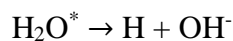
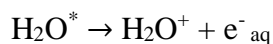
2.2 Biological and Chemical effects of Radiation

Chemical and physical changes in irradiated water

Ionizing radiation produces secondary electrons which in turn deposit their kinetic energy throughout a water volume; this is relevant when studying mammalian tissue which is constituted of approximately 70-85% water.[8] Initially, physical changes take place once the radiation interacts with the water volume creating energetically ionized molecules, H_2O^+ , H_2O^* , and free electrons within 10^{-15} seconds.[9] In the window of 10^{-15} to 10^{-12} sec, these three species induce changes within the volume producing free radicals.[9] The ionized water molecule reacts with a neighboring water molecule forming a hydronium ion and a hydroxyl radical:



The excited water molecule can transfer its energy through two processes, either by losing an electron thereby becoming an ion or by molecular dissociation:



The free electrons lose energy through vibrational and rotational excitation of water molecules and become thermalized within 10^{-12} sec.[9] The thermalized electrons are then captured by surrounding water molecules that orient their permanent dipole moments and becoming a cluster or aqueous electron. Of these four chemically active species, three of these, OH^- , H_2O^+ and e^-_{aq} , are reactive due to their unpaired electrons. These radical species are also known as free radicals and can be responsible for biological damage. Due to cells being made of 80% water, these free radicals cause a great deal of the DNA damage, as much as two thirds of the DNA damage when the cells are exposed to both ionizing and non-ionizing radiation, specifically low LET (<2 keV/ μm) radiation (x-rays or gamma rays). [22]

Biological Effects of Radiation

Radiation damage to biological cells occurs due to both direct damage and indirect damage.[5] Direct damage is a result of the radiation itself interacting with the cells components, for instance where proton radiation creates ions that physically break base pairs in the DNA strand or both of the DNA phosphate backbones otherwise known as a single or double strand break, respectively. These, in addition to other types of changes in the DNA structure (i.e. point mutations, crosslinks between strands, or chromosome aberrations), if not repaired can lead to cell damage, apoptosis (programmed cell death), or necrosis (death due to injury).[5] Direct damage is the primary reason for cell death when the cells are exposed to high LET (> 4 keV/ μm) radiation (i.e. protons, neutrons heavy ions). Direct damage to DNA due to high LET radiation is difficult to repair and the process is challenging to modify by chemical or physical means. [22] Indirect damage takes place due to chemical reactions with free radicals created by the radiation interaction with the biological material, an example being where an OH^- radical attacks a DNA sugar resulting in a single strand break. Double strand breaks can be caused by a

single radiation track by both high and low LET radiation or multiple breaks caused within a close proximity (within 6-10 base pairs) to the break termini.[23]

The biological effects of dose can vary widely according to dose, type of radiation and observed timespan. Some effects can be immediate while others can take years to manifest. Generally, these effects are categorized as either stochastic or non-stochastic.[9] There is no definite determination that the effect will be present, an example of that effect being cancer. A large population of individuals can be exposed to radiation, however, they may not all develop cancer in their lifetime. In addition, since cancer can occur naturally without exposure, it is not guaranteed that any radiation exposure is the cause of the incidence of cancer. Rather, the odds of cancer incidence increase with radiation exposure dose and there is no threshold dose under which there is zero probability of developing cancer. Shortened lifespan, genetic effects and mutated offspring are possible stochastic effects of ionizing radiation. Non-stochastic effects, in contrast, have a clear causal effect with dose and have a threshold dose.[9] Skin erythema, infertility and cataracts are examples of non-stochastic effects as well as acute radiation syndrome, or ACR.[9] ACR can develop when a person receives a single, large, short-term whole body dose of radiation causing a depletion of radiosensitive cells in the blood and digestive tract. This can cause bone marrow damage, infection and at high doses, death.

2.3 Radioprotectors

To delay or prevent the effects previously discussed, there are methods including incorporating shielding, reducing time of exposure and increasing the distance between the source and the individual to protect individuals who are exposed to radiation. In those cases where the individual may not have practiced these safety procedures, it may be necessary to use radioprotectors to reduce or eliminate the effects of ionizing radiation. An ideal radioprotector would provide: significant protection against radiation effects, a general protective effect on the majority of internal organs, an acceptable route of administration, an acceptable toxicity and stability profile, an effective time-window effect, and must be compatible with a wide range of other drugs available to patients and personnel. [4] While there is no radioprotector that satisfies all of these conditions, there are those that are able to provide some protection from the effects of indirect damage from radiation.

Amifostine and other Synthetic Radioprotectors

The current gold standard used is WR-2721, otherwise known as amifostine, a prodrug meaning it must experience a chemical conversion through metabolic processes before becoming an active compound. It is administered in a pharmacologically inactive form.[15] Once the thioester bond is cleaved by a phosphatase within the normal endothelium yielding a free thiol, the active free radical component of amifostine can permeate the cell membrane.[24] The active molecule, WR-1065 in thiol form, has shown to provide radioprotection for cells preventing death in the presence of both direct and indirect ionizing radiation as well as mitigating the effects of genomic instability for the surviving cells. [25, 26] Amifostine can also protect by binding to free radicals allowing for detoxification, enhance DNA protection and repair, and induce hypoxia, preventing reactive oxide radicals from forming.[27, 28] Its effectiveness as a

radioprotector has allowed it to be used in industry, medical and government applications, including as a safety precaution for astronauts on previous missions to the moon in case of a solar event. It is the most widely used cytoprotective compound approved by the Food and Drug Administration as a radioprotector. [22, 25] However, amifostine is not without drawbacks. It must be administered by trained personnel, which in the case of a nuclear disaster or attack could be problematic. Gaining access to large amounts of the compound as well as gathering a sufficient medical staff to administer the drug might face considerable problems. Also, side effects are possible with amifostine including acute hypertension, severe nausea, vomiting and allergic reactions.[18] In addition, amifostine is unable to provide protection for all the human organ systems, the central nervous system is completely unprotected due to the inability of the drug to pass the blood-brain barrier. [29] As mentioned before, a beneficial time-window effect is necessary for an ideal radioprotector but with amifostine, it must be administered before exposure to maximize its effect, which could be next to impossible in the case of a nuclear accident or terrorist attack. Finally, the cost of amifostine does not make it a viable option to the population at large with a minimum price tag of \$1000. [30] While amifostine is useful in certain situations, it is necessary to find other potential radioprotectors that better satisfy the conditions of an ideal radioprotector.

Palifermin is a radiomitigator, meaning it is delivered after radiation exposure, but before the manifestation of normal tissue toxicity, in an attempt to prevent or limit the expression of radiation-induced side effects.[28] Radiomitigators primarily target the series of cellular recognition/repair responses initiated after radiation exposure, including DNA repair, apoptosis activation and the cell proliferation and immunoinflammatory responses. Palifermin is considered a prototype mitigant.[28]

Nitroxides are stable free radical compounds that have been shown to interact with other free radicals such as those that arise from ionizing radiation. Tempol is an example of a nitroxide that has demonstrated protective properties *in vitro* for mammalian cells against cytotoxicity from radiation in aerobic conditions as well as *in vivo* after whole body irradiation.[31, 32] Nonetheless, similar to amifostine, tempol has potential side effects such as hypotension and seizures at doses required to operate at full potential as a radioprotector and it has a limited time window.[4]

Bisbenzimidazol compounds, specifically Hoechst 3342, have been shown to be radioprotectors *in vivo* with an intravenous administration half an hour prior to a single dose of radiation of 12 Gy in mouse lung model. [33] However, Hoechst 3342 shows cytotoxicity and mutagenic effects at higher concentrations so efforts are being made to explore derivatives of Hoechst that show less of a negative effect. [34]

Natural Radioprotectors

Cytokines are another group of radioprotectors that consist of a group of soluble glycoproteins and low molecular weight peptides that stimulate cell proliferation and differentiation between hematopoietic and lymphoid tissues.[35] The most extensively researched cytokine as a potential radioprotector is Interleukin-1 (IL-1). IL-1 is produced by monocytes and macrophages in response to the presence of toxins, other cytokines, and microbial and viral agents. [35] Cytokines have shown potential as a viable radioprotector but they do have cytotoxicity effects which have encouraged researchers to discover a non-cytokine drug that can perform the same function. Immunomodulators have been shown to increase cytokine activity which can stimulate growth, differentiation and proliferation of stem cells. They seem to protect and repair the hematopoietic system through a greater production of bone

marrow cells which in turn produce more lymphocytes, platelets and granulocytes.[36]

Immunomodulators are promising in protecting the hematopoietic system but unfortunately do not protect other organ systems and are not generally available to the public. Furthermore, as seen with many other radioprotector drugs, it must be administered by a professional intravenously which causes problems in cases of nuclear accidents and attacks.

Many natural antioxidants and herbal medicines have shown some potential in providing radioprotection of biological tissue. Vitamin E is free radical scavenger, shows low toxicity even at high doses and is naturally occurring. [37] Vitamin E has been shown to be effective in improving survival rates when injected into mice exposed to radiation but showed no effect then taking the same dose orally.[38] It also shows a lower dose reduction factor (DRF) than amifostine. Dose reduction factor is determined by dividing the dose of radiation in the presence of the drug by the dose without the drug present to cause a set lethality e.g., a lethal dose to 50 percent of the population after 30 days (LD 50/30). Therefore, it still does not take as large a dose of radiation to cause biological tissue death with vitamin E present as it takes when amifostine is present. Melatonin is hormone produced in the pineal gland that is used as an over-the-counter (OTC) sleep aid and studies have suggested that it is capable of scavenging free radicals [39] but has shown to have side effects such as sleepiness and hypotension and also interacts with nifedipine, a hypotension drug, intensifying the effect.[40] Ginseng, a popular OTC herbal medicine, lauded for its benefits for improving aging, diabetes, reducing stress and fatigue and promotion of DNA, RNA and protein synthesis. [41-43] Human lymphocytes treated with ginseng extract were exposed to radiation and showed a reduction in micronuclei, an indicator of cellular DNA damage. [44] Further studies are necessary to determine the toxicity of ginseng and its derivatives as a potential oral delivery antioxidant.

A very promising area of natural radioprotectors is soy and soy products. Consumption of soy products has shown to reduce risk of cardiovascular disease and reduced the chances of bone loss in postmenopausal women.[45-47] Genistein, a naturally occurring compound in soybeans, shows benefits in improving cardiovascular disease, high cholesterol and osteoporosis. [48] It has also shown promise as a radioprotector, increasing survival rate when intravenously injected into mice 24 hours in advance of being subsequently exposed to gamma radiation.[49] However, no effect was determined in the same experiment when injection took place 1 hour before exposure. While it shows to have radioprotection properties for normal cells, it has also shown radiosensitizing properties in regards to tumor cells, particularly human cervical cancer cells.[50] Genistein has shown ability to inhibit growth of different cell lines and reduce viability with an enhanced effect when combined with radiation.[51] While it shows a growth inhibitory effect at genistein concentration doses greater than 10 μM , it stimulates growth at doses below the same value. One study observed the effects of different doses of genistein between 0.01-100 μM on human breast cancer carcinoma cells with low doses from 1-10 μM showing growth promotion while inhibition was displayed at higher doses. [52]

Cerium Oxide Nanoparticles

In recent years, nanotechnology has come to the forefront of biomedical research with applications in drug delivery systems, luminescent biomarkers, tissue engineering as well as many others. [53] One specific application, cerium oxide nanoparticles (CNPs), has shown great promise as a radioprotector and radiosensitizer. CNPs consist of a cerium core surrounded by an oxygen lattice and are synthesized using a micro-emulsion process consisting of surfactant sodium bis(2-ethylhexyl) sulfosuccinate (AOT) toluene, and water.[20] The CNPs exhibit regenerative antioxidant properties in the reaction cycle of Ce^{3+} to Ce^{4+} to Ce^{3+} which continues

on the surface of the CNPs providing antioxidants with unique protection properties.[54, 55] Cerium oxide can be designed to retain a specific Ce^{3+}/Ce^{4+} ratio which when controlled can determine its distinction as an effective catalase mimetic, superoxide dismutase (SOD) mimetic, or both, cleaving O_2 radicals and hydrogen peroxide and rendering them inactive.[56-58] They have shown other antioxidant behaviors including nitric oxide scavenging [59] and hydroxyl radical scavenging [60]. In contrast, CNPs have also shown oxidant behaviors as well under certain environmental conditions.[61] Both properties have proven beneficial in research of the effects of CNPs on normal cells as well as cancer cells. CNPs have been shown to possess an inherent cytotoxicity to cancer cells as well as the ability to sensitize tumor cells to radiation induced apoptosis while protecting the surrounding healthy tissue. [17, 20, 62-64] It is not well understood for the cytotoxicity to tumor cells but it is theorized that the CNPs provide free radicals that increase oxidative stress to the tumor cells. Not only have they shown cytotoxicity towards cancer cells, studies have shown them to limit the invasive characteristics of tumor cells. In one study, they reduced the ability of myofibroblasts to induce invasion by squamous tumor cells and also restricted the inherent ability of squamous tumor cells to invade without the presence of myofibroblasts stimulation. [65, 66]

The dual impact of CNPs as an oxidant for cancer cells as well as an antioxidant for normal cells makes it an ideal candidate for radiation therapy especially since studies have shown that natural antioxidants can be dangerous to cancer patients who are currently receiving treatment.[67] In several studies, when treated with CNPs prior to radiation therapy, cell damage and death were decreased for normal tissue in the gastrointestinal (GI) tract [62], lung [20], and head and neck [68]. In contrast, when treating certain cancer cells with CNPs in low pH conditions before radiation therapy, tumor cell death was enhanced. A recent study has shown

the ability of CNPs to drive radiation induced oxidative species in pancreatic cancer cells to higher levels.[69] These results show that CNPs can radiosensitize cancer cells by encouraging production and maintenance of reactive oxygen species (ROS) and maintaining their levels within tumor cells. Combined with their direct toxic effects, CNPs show potential as a very effective weapon against tumor cell viability and growth.

Extending beyond cancer treatment, CNPs show promise in treating other diseases characterized by ROS accumulation. Neurodegenerative diseases such as Huntington disease, Parkinson's disease, Alzheimer's, and age related macular degeneration have been linked to increased levels of ROS which can prevent cellular mechanisms from combating oxidative stress.[70] The impact of CNPs on such diseases have yet to be fully explored, however, preliminary studies have shown they scavenge ROS in mouse models of hereditary retinal degeneration, preventing retinal deterioration and reducing apoptosis in photoreceptor cells. [71] CNPs have also demonstrated the ability to induce the regression of pre-existing pathologic retinal neovasculature suggesting an antiangiogenic property to CNPs, another valuable benefit to add to the long list. [70] In regards to diabetes, increased ROS, especially in the liver where free radicals are removed from the bloodstream, has been recognized as an important factor in the progression of the disease. [72] CNP treatment of diabetic rats has allowed hepatic ROS levels to return to levels comparable to non-diabetic rats as well as decrease triglycerides and increase HDL in the blood. [72] CNPs have also shown to increase the viability of pancreatic islet function increasing insulin secretion and decreasing ROS levels in isolated, cultured pancreatic islet cells. [73] Both studies show the great promise that CNPs have in not only treating diabetes but curing it as well.

While CNPs have shown an apparent lack of toxicity in animal models, studies demonstrate conflicting evidence in regards to cells *in vitro*. This conflict is attributed to as yet undetermined cellular and environmental factors that influence both the oxidant and antioxidant behavior of CNPs. They have found to be toxic to bronchial epithelial lung fibroblasts in culture [74], yet non-toxic to mammary epithelial cells [17], macrophages [75], keratinocytes [76], and pancreatic cells [69]. In normal cells, the pH level of the cellular environment enables the CNPs to perform radical scavenging. Other studies show that CNPs are toxic to several types of human cancer cells *in vitro*, including squamous cell carcinoma [65], alveolar epithelial cancer cells [64], and pancreatic carcinomas [69]. They also show toxicity to pancreatic tumors *in vivo* reducing the tumor volume by almost 40%. [69] As mentioned earlier, this cellular toxicity is attributed to the ability of CNPs to increase levels of ROS and maintain them within the tumor cells. Despite the conflicting evidence of CNPs' effect on cells *in vitro* and the evidence of toxicity in *in vivo* studies, their ability to behave as both an oxidant and antioxidant for tumor cells and normal cells, respectively, demonstrates the need for further research of CNPs. While many current radioprotectors are characterized by one antioxidant scavenger for every radical to be scavenged, a single CNP particle can scavenge many free radicals and can induce oxidation of many targets through its auto-regenerative capability and their regenerative antioxidant properties prevent the need for multiple treatments. [71] As is evident, CNPs can have widespread influence in biomedical applications.

2.4 Hypothesis and Specific Aims

Radiation exposure is progressively becoming a concern to the general population as evident by past nuclear accidents and disasters as well as the threat of terrorist attack.[77] In addition, as mankind sets sights on deep space travel, an effective radioprotector will be necessary to protect astronauts from the overwhelming amount of radiation associated with deep space.[78] Radiation therapy is always in need of solutions for improving tumor cell kill while protecting normal cells in greater amounts and reducing negative side effects. Amifostine and Palifermin, a radiomitigator, are currently the only FDA approved radioprotectors but they have significant drawbacks in their effectiveness to the general population. Amifostine requires treatment before radiation exposure takes place, has a short half-life (<1 hr.), is quite expensive and has toxicity issues.[79] CNPs show great promise in the areas that remain drawbacks for amifostine. It is the objective of this study to determine the effectiveness of CNPs in protecting human breast epithelial cells when they are exposed to heavy charged particle radiation by measuring the cell survival and determining the DNA damage. These effects will be compared with the effects of those of WR-1065 with a human breast epithelial cell line representing a normal cell population. To accomplish this, three specific aims have been developed.

Specific Aim 1

The first aim of this study was to design and develop a system to irradiate the A184 epithelial breast cell line using a proton beam. This required a beam imaging system in order to characterize the beam by measuring the flux and flux uniformity to determine the dose to the cells.

Specific Aim 2

The second goal was to develop a cell survival curve of the A184 cell line, irradiate the cells both with and without the CNP's and compare the two conditions to determine their radioprotective effectiveness. This was measured by a methylthiazol tetrazolium, or MTT assay, a colorimetric assay that measures the conversion the yellow dye to a purple derivative. The radioprotective effects of the CNP's were also be compared to the current gold standard, amifostine, in the form of its active component WR-1065.

Specific Aim 3

The third goal was to perform DNA damage assays on all cells exposed to CNP's as well as those that are not exposed to determine the cell damage caused by the proton beam as well as the influence of the CNPs in regards to protecting the cells from heavy charged particle radiation. A discussion of the results includes possible theories to explain the mechanisms in which the CNPs influence the normal cell line in the presence of charged particle radiation.

Chapter 3: Materials and methods

3.1 Research Design

The Atomic Physics Laboratory at East Carolina University provides a 2 MV tandem Pelletron accelerator that produces particle beams of various energies and charge states to study atomic collisions.[80] The accelerator produces an ion beam that proceeds through various focusing and steering components to be directed toward an exit point covered with a thin titanium foil where the beam will interact with a cell tray containing the target cells. The target cells are exposed to a predetermined dose and then analyzed for cell survival and DNA damage.

Accelerator System and External Beamline at ECU

A schematic of the accelerator system used at ECU is shown in Fig. 3.1. A general Ionex Corporation model 860A cesium-sputter ion source is used to produce various atomic and molecular ions and is capable of producing negative ion beams in the microampere range as described by Middleton. [81, 82] The production of the wide range of ions that can be produced and their relative abundances have been described in previous literature.[83] For this study, H⁻ ions are produced by the ion source from a TiH cathode and then accelerated by a 30 kV potential along a 1 m acceleration region. A sample diagram of an ion sputter source is provided in the literature.[83] The H⁻ ions are momentum selected by an inflection magnet and then injected into a 2 MV tandem Pelletron accelerator, model 6SDH-2 from National Electrostatic Corporation.

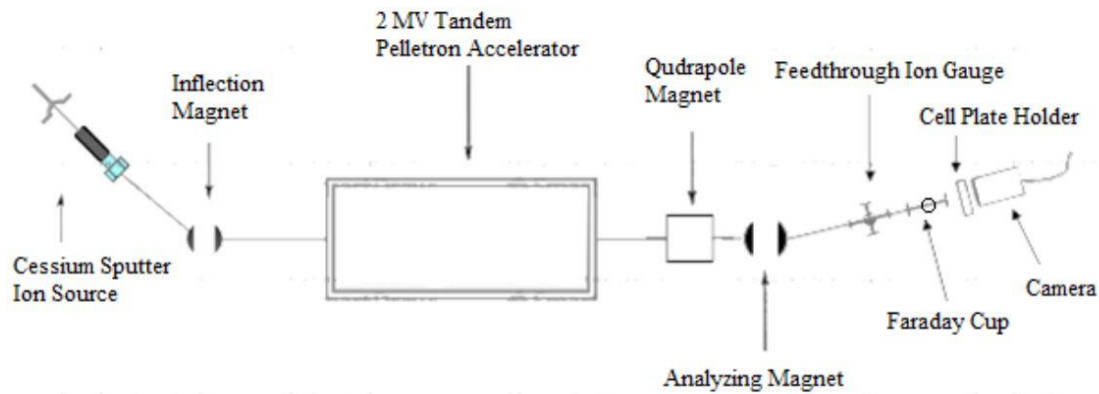


Figure 3.1 ECU Particle Accelerator layout (not drawn to scale)

Previously, the ECU accelerator lab used a tandem Van De Graff accelerator for nearly 4 decades until 2009 when a National Science Foundation grant was awarded to fund the purchase and installation of a new 2 MV Pelletron tandem accelerator. Renovations began in 2010 to expand the lab to house the larger accelerator and expanded beamlines and concluded with its installation in 2012. The Pelletron accelerator is an electrostatic accelerator with a metal and ceramic accelerating tube, two Pelletron chains, and a gas stripping system encased in a pressurized tank that contains up to 550 kPa of SF₆ of insulating gas to prevent discharge. To produce the ion beam, a cesium ion source is heated creating cesium vapor which is released in an enclosure containing a copper cathode and the heated ionizer. Some of the cesium vapor condenses on the cathode while the rest is ionized to become Cs⁺. The cathode is held at a

negative potential, attracting the Cs^+ ions and impacting them on the cathode sample cone (composed of titanium hydride) sputtering H^- ions out of the cone. The cathode is 12.5 mm in length and 10 mm in width with a 1.6 mm well drilled in the center to a 5 mm depth. The well is packed with the TiH powder. Due to the shapes of the potential surfaces defined by the cathode and ionizer potentials, these ions are focused into a beam while other ions including the Cs^+ ions are scattered. Details of the cathode configuration are provided in the literature.[83] The beam is extracted by an extraction potential V_s and focused with an electrostatic Einzel lens, a device that varies electric fields in order to focus the ion beam using ion optics.[84] The beam is momentum selected by the inflection magnet and then is focused using another Einzel lens followed by a pair of electrostatic steerers and injected into the tandem accelerator.

The accelerator creates electric charge by transportation of two Pelletron chains, made of metal pellets connected by insulated nylon links, through a closed pulley system. For a positive terminal Pelletron, a negatively charged inductor pushes electrons off the pellets while in contact with the grounded drive pulley. They retain their charge as they exit the inductor and proceed to the high voltage terminal where the reverse occurs: the chain goes through a suppressor to prevent arcing when coming in contact the terminal pulley on which the positive charge is deposited giving a positive charge to the terminal.[85] The advantage of Pelletron accelerators lies in the fact that they can operate at a higher speed transferring charge more efficiently thus attaining higher voltages. In addition, the chain is more uniformly charged than a Van de Graff belt allowing for a more stable terminal voltage and particle energy. The H^- ion beam is accelerated toward the positive high voltage terminal of the accelerator where they proceed through a stripping gas, N_2 , becoming H^+ ions and accelerated once again to ground potential. This configuration can produce singly charged ions up to 4 MeV which was used for this

experiment along with a 3 MeV beam. More details about the design and operation of the accelerator system are provided in the literature.[80, 86] A pair of quadrupole magnets is positioned after the accelerator, focusing the H⁺ beam followed by an analyzing magnet used to select the beam of the appropriate mass and energy, directing the beam down the left 15° beamline where the target cells are located. A diagram of the 15° beamline is provided in Fig. 3.2.

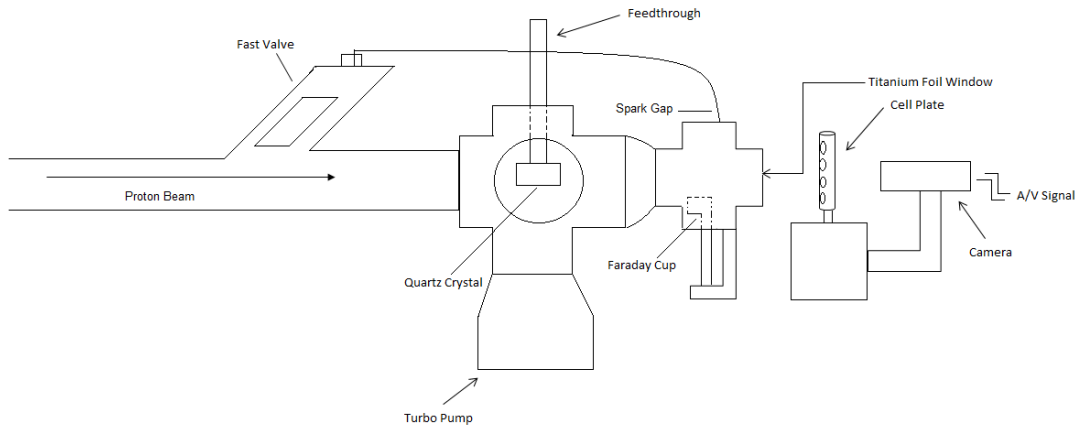


Fig. 3.2 15° beamline side view of irradiation setup

The experimental beamline is pumped by a turbomolecular pump where the pressure is maintained at approximately 10^{-7} torr. Several devices are used to monitor the beamline pressure, beam intensity and beam profile. An ion gauge is used to measure the vacuum pressure by heating a filament which releases electrons that are attracted to a grid held at a positive potential. In their progression toward the grid, they collide with gas molecules creating gas ions. These gas ions are collected with a wire held at a negative potential. The current is measured to determine

the vacuum pressure. A fast shut valve is positioned near the analyzing magnet so that in the case of a sudden loss of pressure due to a foil puncture, the vacuum can be preserved further up the beamline. A quartz crystal is mounted onto a feedthrough block in order to see the beam through fluorescence giving a view of the beam spot through a viewing window on the side of the beamline. Immediately after the feedthrough, a Faraday cup (F.C.) is mounted and used to measure the beam current by insertion into the beam to confirm the number of ions in the beam striking the target.

At the end of the beamline, immediately behind the F.C., a vacuum window consisting of a 12.5- μm -thick titanium foil is epoxied to a brass beamline blank with a 1.4 cm aperture drilled in the center. The window was made as thin as possible to prevent a large loss of energy of the ion beam due to interactions with the nuclei in the foil. With this window thickness, energy loss was determined to be 10% for 4 MeV protons and 15% for 3 MeV protons. Once the beam exits through the foil, it goes through 3.2 cm of air before irradiating the cells contained in a single layer of cells in a single well in the center of a 48 well microtiter plate. The microtiter plate is held in place by two brackets that are secured to a Teflon stand with a reservoir to catch and hold any excess growth medium that may exit the cell plate. The setup is shown in Fig. 3.3.

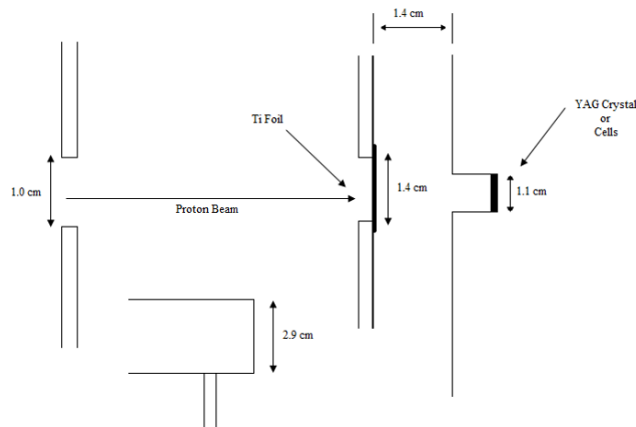


Fig. 3.3 End of Beamline setup

Beam Dose Calculation and Profiling

In order to determine the correct dose to the cells, the beam must be profiled and characterized using information provided by the F.C. at the end of the beamline positioned directly in front of the beam window as well as an yttrium aluminum garnet (YAG) scintillation crystal secured in the cell plate well that is positioned directly in front of the titanium exit window. The dose is calculated using Eq. 2.3, with the fluence rate of the proton beam provided by the beam current measured using the F.C. and the stopping powers predicted by Stopping and Range of Ions in Matter (SRIM) code.[21] The SRIM code calculates the stopping and range of ions into matter at energies up to 2 GeV/amu using a quantum mechanical treatment of ion-atom collisions. This calculation makes use of statistical algorithms which take into account calculated ion collisions and averages the results over the intervening gaps. A detailed description of this calculation is provided in the literature.[21] The SRIM program is able to provide stopping powers for a wide range of types of matter including those used in this experiment, specifically titanium, air and human epithelial cells.

The LET of the beam was first calculated in order to determine the energy loss of the beam as it traveled through each material. The LET equation used is

$$LET = \left(-\frac{dE}{\rho dx} \right) * \rho \quad (3.1)$$

which is then used in to determine the energy loss of the beam as it exits each material thickness

$$\Delta E = E_0 - (LET * \Delta x) \quad (3.2)$$

providing the energy value to determine the next LET value as the beam travels through the subsequent materials in its path. Once the beam exited the 12.5 μm thick titanium window, it traveled through approximately 3.2 cm of air into the single layer of epithelial cells with an assumed thickness of 5 μm , consistent with other similar studies. [87-89] The assumed thickness was an simplification of the true conditions where cells vary in size in shape in true conditions although in regards to the relative dose to the cell, this estimate was not critical and was sufficient for dose calculations. After determining the energy loss due to the exit foil and air, the incident energy was approximately 1 MeV less than the beam energy in the beamline prior to exiting the foil.

After calculating the energy loss through the various materials, the dose is calculated relative to the midpoint of the cell. The dose rate at the midpoint of the cell is calculated with the following equation

$$\dot{D} = \text{Fluence Rate} * \text{Mass Stopping Power} * 1.6 * 10^{-7} \quad (3.3)$$

Dose rate is measured in Gy/sec, fluence rate is measured in $\text{cm}^{-2} \text{sec}^{-1}$ and mass stopping power is measured in $\text{MeV} * \text{cm}^2 / \text{mg}$; $1.6 * 10^{-7}$ is a conversion factor to convert MeV / mg to Gy (J/kg) the standard unit of dose. Calculating the dose rate at the midpoint of is consistent with previous

studies as a standard.[89-91] The cells were irradiated for the correct time according to the prescribed dose.

To ensure proper beam irradiation of our cell sample, the beam was characterized using an yttrium aluminum garnet (YAG) crystal. The crystal scintillates when exposed to charged particles which gives the position of the beam spot relative to the cell sample. The YAG crystal was secured in a sample microtiter plate with same well count as the plates in which the cells were seeded, specifically the E5 well. Due to the orientation of the wells on the plates, a 180 degree rotation of the plate places the B4 well directly in the path in the beam, allowing for two irradiated cell wells per plate. A camera was attached directly behind the cell plate holder focused on the well containing the YAG crystal capturing an image using XCAP® for Windows that is then characterized using ImageJ, a public domain, Java based script program developed at the National Institute of Health.[92] The image is processed and portrayed in a 3D image that gives variations in the scintillation of the crystal, representing the variability in the beam flux on the YAG crystal. The beam is adjusted using the previously mentioned quadrupole magnets until the beam is uniform with estimated <5% variation across the YAG crystal. A sample 3D image representing the beam flux is shown in Figure 3.4.

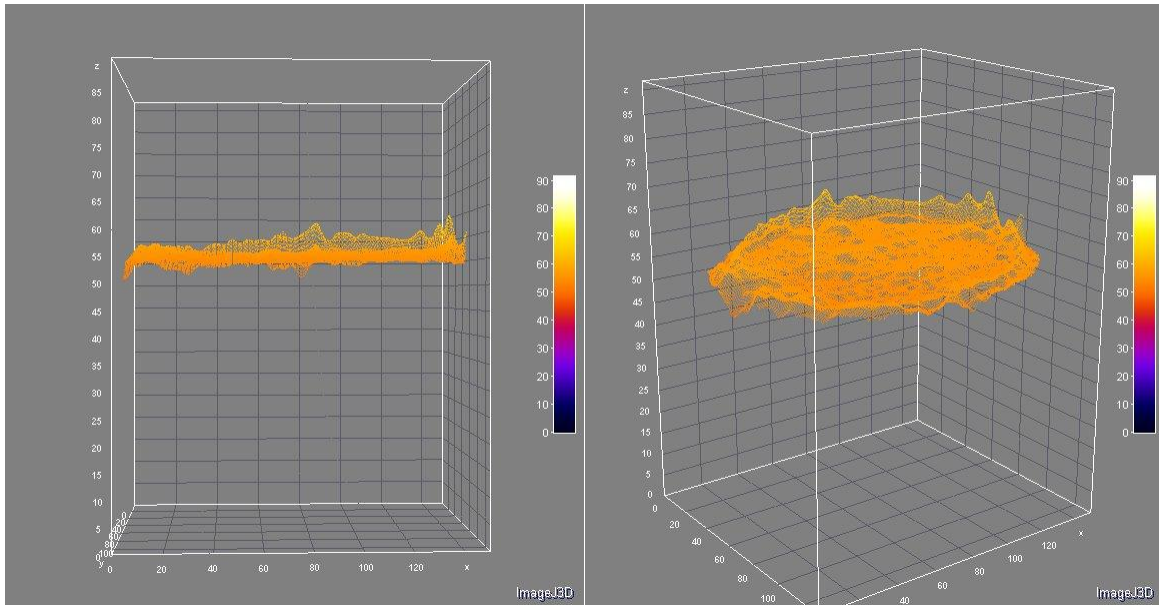


Fig. 3.4 Sample Beam Intensity Image on ImageJ software (side view and top view)

Cell lines and Culture Conditions

The experiment model used for the non-tumorigenic cell line in this study is the A184 epithelial breast cell line(ATCC[®] PCS-600-010).[93] The cell culture procedure was used in previous CNP research involving x-ray radiation.[20, 62] The stock cultures were maintained in 75 cm² culture flasks in Mammal Epithelial Basal Medium (MEBM) complete media (minus gentamycin-amphotericin B) purchased from Lonza[®] supplemented with 1 ng/ml cholera toxin and 0.005 mg/ml transferrin and incubated at 37° C in a 5% CO₂ environment. The cholera toxin stimulates cell growth and the transferrin is an important extracellular antioxidant preventing the production of free radicals by binding iron, a free radical catalyst.[94] For experiments, the cells were washed with 10 ml of phosphate-buffered saline (PBS) solution for several seconds to remove any residual media. The PBS was aspirated and the cells were trypsinized with 3 ml of 0.25% Trypsin/EDTA (Ethylenediaminetetraacetic acid) solution (Invitrogen/Life Technologies,

Inc.). The cells were then incubated for 15 minutes at 37° C with 5% CO₂ until the cells were rounded and had detached from the flask wall. The cell suspension was then added to a 15 ml centrifuge tube and 9 ml of media were added to dilute the trypsin. The cells were spun at 150 x g for 10 minutes at 4° C and then were re-suspended in 3 ml of MEBM media. One ml of the cell suspension was added to a new 75 cm² flask with 15 ml of media to produce a new stock culture. The remaining 2 ml were used for plating cells for experiments. For cell counts, 100 µL were removed from the remaining cell suspension. Of this, 50 µL were removed and placed into an Eppendorf tube with 50 µL 0.4% trypan blue. After mixing, 10 µL were immediately loaded into a hemocytometer and trypan-blue excluding cells in four 1 mm² sectors were counted. An example of the cell counts for all four sectors would be 74, 89, 82 and 76 giving an average of 80 cells. This number is then doubled to account for 1:2 dilution in the trypan solution, giving a number of 160 x 10⁴ cells/ml. The desired number of cells per well in a 48 well microtiter plate were 4 x 10⁴ cells in a total volume of 200 µL solution meaning that the dilution would require 20 x 10⁴ cells/ml. The dilution factor would therefore be

$$1.6 \times 10^6 / 20 \times 10^4 = 8$$

Therefore, 1.0 ml of cell solution were added to 7.0 ml media giving a 1:8 ratio of cell solution to media. Wells B4 and E5 were seeded for irradiation and wells B1 and C1 were seeded for controls in a 48 well microtiter culture plate with 200 µL of the 20 x 10⁴ cells/ ml suspension. Wells B1 and C1 were seeded with 200 µL of cell solution as non-irradiated controls and wells B8 and C8 were seeded with 200 µL of cell solution as non-irradiated CNP control when required for a particular experiment. This allowed for comparison between the non CNP control and CNP control for possible toxicity. CNPs were added in a total volume of 50 ml (see below).

The plates were incubated at 37° C with 5% CO₂ for 24 hours to allow the cells to grow toward confluence.

CNP and WR-1065 Preparation

The CNP synthesis is described in detail in the literature.[20] Several methods exist for the synthesis of stable nanoceria involving a hydrothermal process or precipitation and re-dispersion techniques that do not produce surface active nanoceria particles. To retain surface active states and ensure non-toxicity, controlled room temperature techniques that can yield a nanosuspension in a one pot reaction are necessary.[95] Therefore, nanoceria must be synthesized in water soluble, biocompatible mediums to retain surface activity over a diverse range of pH and cellular environments. [95]

The CNPs for this experiment were synthesized using several different methods to achieve different effects when exposed to the cells and subsequent irradiation and were manufactured at Burnett College of Biomedical Sciences and Advanced Materials Processing and Analysis Center and the Mechanical, Materials and Aerospace Engineering, and Nanoscience and Technology Center (NSTC), University of Central Florida in Orlando, FL. Due to the proprietary nature of the CNPs, only three methods will be described here. [96] Method 1 uses the microemulsion process comprising surfactant sodium bis(2-ethylhexyl) sulfosuccinate (AOT), toluene and water. The AOT is dissolved in 50 mL of toluene and 2.5 mL of 0.1 M aqueous cerium nitrate solution is then added and stirred for 45 minutes. After stirring, 5 mL of 30% of hydrogen peroxide is added was then added by drop method. The reaction takes place for one hour and then the mixture is left to separate into two layers, the upper layer consisting of toluene containing non-clustered ceria nanoparticles and the lower level the aqueous phase. The CNPs are precipitated by addition of 30% ammonia solution and washed with acetone and water to

completely remove the surfactant. The CNP's are then suspended in deionized water at a 5 mM concentration.

Method 2 synthesizes a higher surface Ce^{3+} CNPs using simple wet chemical procedures. Cerium nitrate hexahydrate is dissolved in deionized water and then filtered using a 20 nm filter to remove undissolved impurities and is then oxidized using hydrogen peroxide and stirred overnight.[54, 60, 95] The CNPs can be dialyzed against DI water to remove excess oxidizers and nitrate ions from the solution. Method 3 is similar to method 2 with the difference being ammonium hydroxide is used instead of hydrogen peroxide is used to form the CNPs with a higher surface Ce^{4+} concentration. The CNPs manufactured with method 2 are 3-5 nm in size while the method 3 CNPs are 5-8 nm in size.

The CNPs are characterized using x-ray photoelectron spectroscopy (XPS) and high-resolution transmission electron microscopy (HRTEM). The resulting nanoparticles are ultrafine in the range of 2-5 nm, uniformly distributed and have nanocrystallinity.[17, 97] The XPS spectrum shows the presence of a mixed valence state with Ce^{+3} and Ce^{+4} peaks and is provided in the literature.[17] The Ce^{+3} are present in the crystal lattice due to oxygen vacancies created by the surface chemical reactions. [98]

The WR-1065 preparation was done according to a similar experiment referenced in the literature.[25, 26] WR-1065 was obtained from Sigma-Aldrich®. Immediately before treatment, WR-1065 was dissolved at a concentration of 20 mM in phosphate-buffered saline (PBS) and then filter sterilized. 50 μ L were added to the cells 60 minutes prior to irradiation for final concentration 4 mM.

3.2 Cell Survival and DNA damage assay

24 hour after seeding, the cells were treated with the CNPs. Serial dilutions of a 5 mM stock were made according to the required concentration for treatment. One ml of the 5-mM concentration was added to 9 ml of media lacking phenol red (clear media) for a 1:10 solution, and then subsequent dilutions were made down to a 500-nM concentration. Then the desired concentration is added to the plates. For example, if the desired concentration was 1 μ M concentration, then 50 μ L of the 5 μ M CNP solution is added to the 200 μ L of media in the cell well giving a 1:5 dilution and resulting in a final concentration of 1 μ M. The concentrations tested throughout this research were controllably varied from 100 nM to 10 μ M. After addition of the CNPs, the cell plates were incubated for another 24 hours.

On the day of irradiation, the media was aspirated and the cell wells were washed with 100 μ L of media. For the WR-1065 experiments, 50 μ L of a 20 mM stock was added for a final treatment concentration of 4 mM one hour before irradiation. Prior research indicates this is the ideal exposure time for maximum cell protection.[25, 26] Due to the cytotoxicity of WR-1065, a 24 hour exposure similar to the CNP concentration was not feasible. The media was then aspirated and the plates were transported to the accelerator lab where they were mounted on the cell plate holder and irradiated for the required dose. Once irradiation is complete, the plates were then transported back to the cell biology lab and 200 μ L of clear media were added to the cell wells, along with wells A1 and B1 for a background control for the MTT assay. The plates were then returned to the incubator for an additional 24 hours.

3.3 MTT and TUNEL Assays

Twenty-four hours after irradiation, cell viability was assessed using the MTT assay. The MTT assay is a colorimetric assay that measures cell viability by the reduction of tetrazolium salts, particularly for this assay, yellow tetrazolium MTT (3-(4, 5-dimethylthiazolyl-2)-2, 5-diphenyltetrazolium bromide). When MTT is reduced by metabolically active cells by dehydrogenase enzymes, the resulting intracellular purple formazan can be quantified using spectrophotometry. The assay can determine metabolic activity and conversely the reduction of said activity due to apoptotic events or necrosis.

44.5 μ L of 5 mg/ml MTT reagent (Sigma-Aldrich[®]) dissolved in PBS were added to the all plate wells that contain media and allowed 2 hours to incubate. The media was then removed being careful to not disturb the purple crystals in each well. The purple crystals were re-suspended in 400 μ L of 100% 2-propanol until they were completely dissolved.[99] The suspensions were then measured for their absorbance at 570 nm wavelength in a Tecan plate reader, model Infinite 200PRO. The absorbance values were recorded and saved in an Excel spreadsheet.

The survival rates were calculated by averaging the absorbance values of the wells that were irradiated, subtracting the averaged absorbance values of the background wells, then that value is divided by the average of the non-irradiated, non-CNP control absorbance values (minus background) and normalized to 1. The standard error is calculated by taking the standard deviation and dividing by the square root of the number of trials. For each experiment, two cell plates were seeded and treated per concentration as well as two cell plates for the irradiated control. P-values were calculated for each experiment using a 2 sample mean t-test to determine

if the difference in cell survival of the CNP treated cells was statistically significant ($p < 0.05$) compared to the irradiated, non-treated control cells.

The degradation of nuclear DNA into nucleosomal units is the defining feature of apoptosis. At the beginning of the process, the chromosomes are cleaved into large fragments after which endogenous Ca^{+2} and Mg^{+2} –dependent endonucleases cleave the chromatin at the linker DNA sites between the nucleosomes, creating DNA fragments. Terminal deoxynucleotidyl transferase deoxyuridine triphosphate (dUTP) nick end labeling, or TUNEL assay is a quantitative and qualitative assay that detects DNA strand breaks by labeling the terminal end of nucleic ends which are identified with terminal deoxynucleotidyl transferase (TdT) that will act as a catalyst for the addition of dUTPs that mark the strand breaks with a fluorescence marker. TdT catalyzes the template-independent addition of deoxynucleotide triphosphates to the 3'-OH ends of DNA. When fluorophore labeled nucleotides are incorporated by TdT, nuclei with degrading DNA can be detected by immunofluorescent techniques. The brighter the fluorescence indicates a higher measure of cell damage, an effective sign of likely apoptosis. A more detailed description of the TUNEL assay can be found in the literature.[100]

To perform the TUNEL assay, cells were seeded in 6 well plates on top of coverslips similar to the earlier process for cell plating with one major difference: in order to maintain the same cell density as for the 48 well plates, the surface area was calculated to be 10 times larger in the 6 well plate as the 48 well plate well, so 10 times as many cells were seeded. 4×10^5 cells total in a total volume of 2 ml were added to the wells and they were incubated 24 hours. 5x CNP stock solutions were added at a 1:5 ratio in the same manner as for the MTT assay and were again incubated for 24 hours. The same method of irradiation was performed for the TUNEL

with the exception of 2 mL of clear media added post irradiation. The plates were then incubated an additional 24 hours.

The TUNEL protocol began with removal of the media and a PBS wash of the coverslips. 500 μ L of 4% paraformaldehyde fixative was added to completely cover the coverslips which were then incubated for 15 minutes at room temperature. Fixative was removed and 2 mL of 0.25% Triton® X-100 permeabilization reagent was added followed by a 20 minute incubation at room temperature. The coverslips were then washed twice with PBS. In order to ensure that the TUNEL assay was effective in marking DNA strand breaks, it was necessary to induce DNA strand breaks in a positive control. The positive control non-irradiated coverslips were fixed and permeabilized with 10 μ L of DNase I diluted in 90 μ L of water for 30 minutes at room temperature. After incubation, the control coverslips were washed with PBS and then subjected to the TdT protocol along with the irradiated coverslips.

The Click-It® TUNEL assay protocol is provided by Life Technologies™.[101] 100 μ L of TdT reaction buffer were added to all coverslips to cover the entire coverslip and then incubated for 10 minutes at 37° C. After incubation, the TdT reaction buffer is removed and 50 μ L of a TdT reaction mixture consisting of the reaction buffer, Ethynyl-dUTP (EdUTP) and the TdT enzyme is added to each coverslip and then incubated for 60 minutes at 37° C. After incubation, the coverslips are washed twice with 3% bovine serum albumin (BSA) in PBS for 5 minutes each. 50 μ L of a Click-iT® Plus TUNEL reaction cocktail is added to each coverslip and then allowed to completely cover the surface. The coverslips are incubated for 30 minutes at 37° C, protected from light. The reaction cocktail is then removed and each coverslip is washed with 3% BSA in PBS for 5 minutes. The coverslips are mounted on microscope slides with a drop of from an eyedropper of 4',6-DiAmidino-2-PhenylIndole (DAPI) a fluorescent stain that

binds to A-T regions in DNA, a common stain used in fluorescence microscopy and is effective in staining of fixed cells. The coverslips are sealed with an adhesive to the slides and then examined with a fluorescence microscope. The slides were examined using a confocal fluorescence microscope brand and model number Zeiss LSM700. The confocal microscope is able to detect several wavelengths simultaneously, two of which are fluoresced in this particular assay, DAPI which fluoresces at 405 nm, and the TUNEL which incorporates an AlexaFluor 568 nm fluorophore that attaches to the nicked-end DNA strand. The DAPI reveals the presence of the DNA with a blue/violet fluorescence while the fluorophore indicates DNA damage with a red fluorescence. The more abundant and brighter the red fluorescence, the more extensive the DNA damage.

Chapter 4: Results

4.1 Dose Adjustments

In order to determine the accurate dose administered to the cells in the plate well, the flux incident on the well surface needed to be determined. While the F.C. gives the total beam current before it exits through the foil window, it measures the total current over an area of approximately 7 cm^2 while the area of the cell well is approximately 1 cm^2 . While the beam area is not as large as the area of the F.C. due to several collimators situated in the path of the beam, it is still collecting both the proton beam and subsequent scatter released as the result of interacting with the collimators. To measure the approximate beam incident on the cell well, a larger YAG crystal with a diameter of 2 cm was placed in the same position of the irradiated cell well and a beam profile was measured. Using ImageJ, a 2D slice was taken from the midpoint of the crystal image and plotted in a beam intensity vs. channel (position) plot. The crystal image and 2D profile is shown in Fig. 4.1. This slice was taken in both the x and y direction (y in the direction of gravity). Based on the orientation, the YAG crystal in the 48 cell well plate was set in the center of the position of the larger YAG crystal. The profile of the smaller crystal was also taken and a length was measured and placed in the center of the larger crystal 2D profile. The intensity in this region was integrated and normalized to the total beam intensity in both the x- and y-direction. To determine the fraction of beam incident on the cell well, the intensity of the smaller beam profile was divided by the intensity of the larger beam well. The percentage of beam incident on the cell well was calculated to be approximately 55 percent of the measured beam current. The other 45 percent was beam scatter caused by the beam exiting the foil window and

scatter due to air. Once the doses were adjusted, the cell survival curves that were measured showed good agreement to previous research of proton irradiation cell survival curves.[89] These results will be discussed later. While the beam energies used were 3 MeV and 4 MeV for the proton beam before exiting the foil, the results will be characterized by the incident beam energy in order to give better understanding of the dose deposition within the cells.

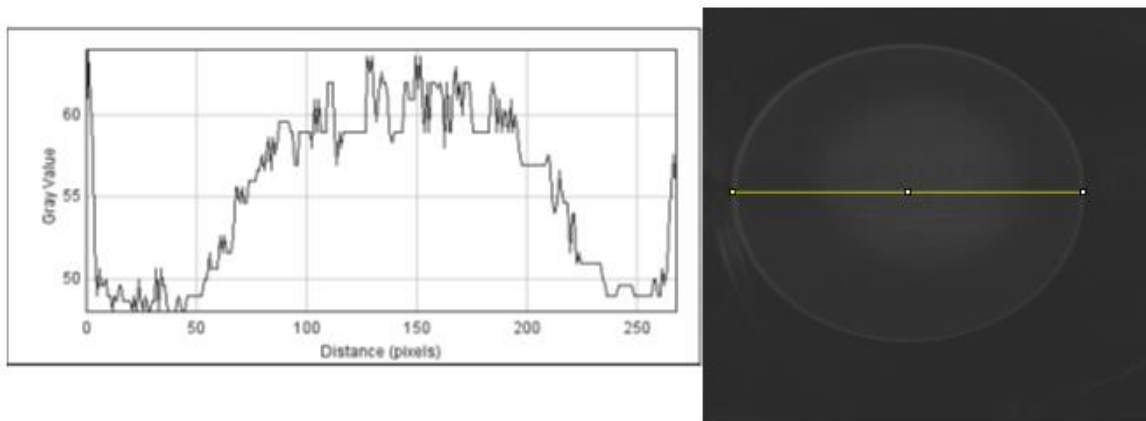


Fig. 4.1 YAG crystal image of beam profile including scatter. The plot shows the beam profile intensity vs. position across the line at the midpoint. The position is measured in pixels.

4.2 CNP survival results with 2 MeV protons

Several CNP types were tested and were all named according to the labels on their vials received from UCF. A typical experimental run would include 2 plates per CNP type and two

plates of irradiated controls with no additives to determine the radiation damage to unprotected cells. Dose was administered in different amounts to see the effect of the CNPs at different levels of damage.

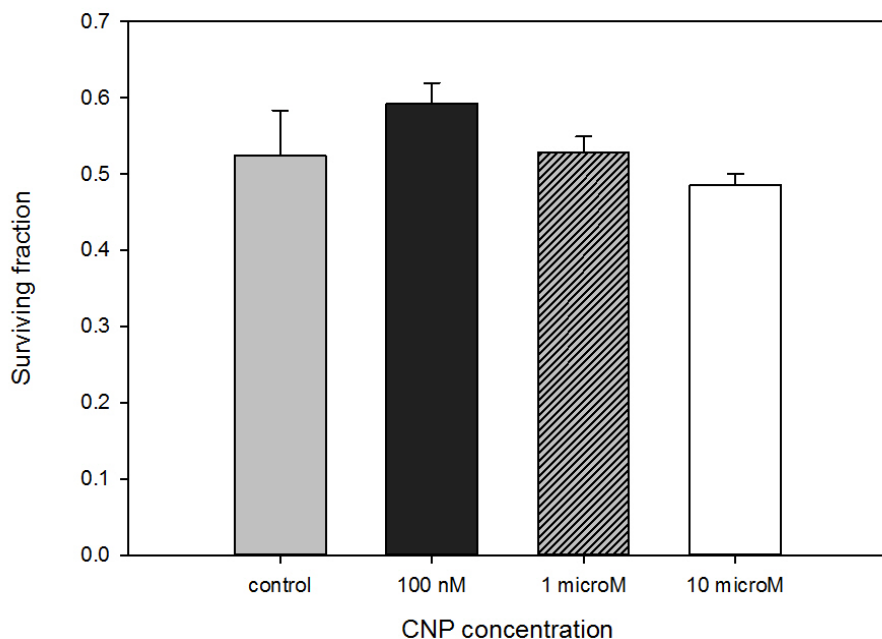


Fig. 4.2 Surviving fraction of A184 breast epithelial cells irradiated with an incident energy of 2 MeV protons for a dose of 1.1 Gy vs. CNP concentration. An MTT assay was used to assess surviving fraction based on metabolic activity. The control represents the irradiated non-treated cells. Error bars represent standard error.

1 Gy Proton Dose Results

The results of the first CNP tested is shown in Fig. 4.2. Since it was the first CNP type, it was the only one received without a label or distinction. Cell survival following exposure at different concentrations was measured at a dose of 1 Gy. As shown in the plot, the 100 nM concentration appears most effective in improving cell survival, however the p-value was 0.37, well above the standard of $p < 0.05$, therefore these results were statistically insignificant. The 100

nM concentration was shown to be effective in previous research with respect to x-rays while the higher concentrations were tested to determine if increased concentration was more effective in improving cell survival.[17]

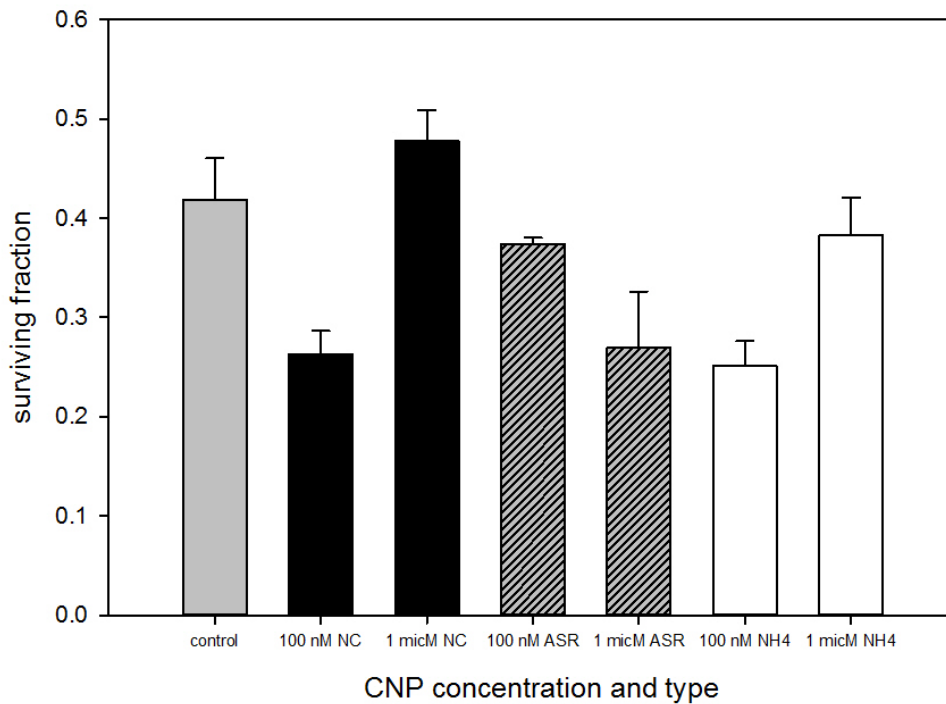


Fig. 4.3 Surviving fraction of A184 breast epithelial cells irradiated with an incident energy of 2 MeV protons for a dose of 1.1 Gy vs. CNP concentration and type. An MTT assay was used to assess surviving fraction based on metabolic activity. The control represents the irradiated non-treated cells. Error bars represent standard error.

The results of exposure to CNP types ASR, NH4 and NC are shown in Fig. 4.3 at a dose of approximately 1.1 Gy. Two concentrations of 1 mM and 100 nM were used to determine if there is any difference in the effect seen post irradiation. The irradiated control showed 42 percent survival while the 1 mM NC treated cells showed a 6% increase in cell survival, however a p-value of 0.26 determines that this increase in survival is not statistically significant. The ASR

and NH4 showed lower survival fractions compared to the irradiated control. It is worth noting that this batch of CNPs were tested in this experiment a month after they were received and recent research suggests that age affects the efficacy of CNPs as a free radical scavenger.[102]

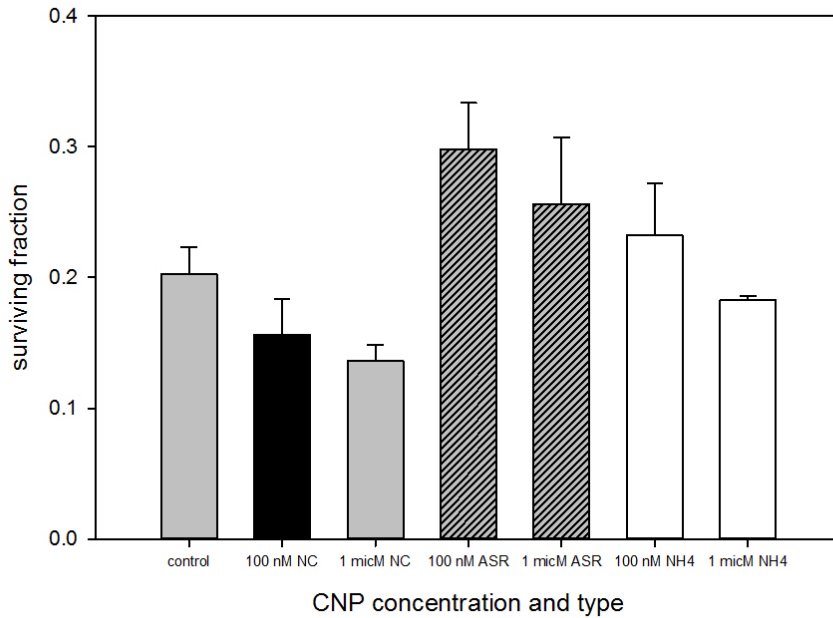


Fig. 4.4 Surviving fraction of A184 non-malignant breast epithelial cells irradiated with an incident energy of 2 MeV protons for a dose of 3.6 Gy vs. CNP concentration and type. An MTT assay was used to assess surviving fraction based on metabolic activity. The control represents the irradiated non-treated cells. Error bars represent standard error.

3 Gy Results

In Figure 4.4, the survival fractions are shown for the three CNP types at a dose of 3.6 Gy. Contrasted to the effects seen at 1.1 Gy, these data showed a lower survival fraction for the control which is expected. However, the set of data displayed a higher survival for both ASR concentrations and for the 100 nM NH4 CNPs with a p-value of .14 which is higher than our

accepted value of 0.05. Also, while the ASR type showed higher survival at lower concentrations as it did for 1.1 Gy, now both the NH4 and NC types have shown a reversal of the trend seen at the lower dose of 1 Gy. It is not clear why but it is thought that the variation of cell plating that is inherent to the technique could be a cause. An alternative method could improve the consistency of the cell counts and is discussed later.

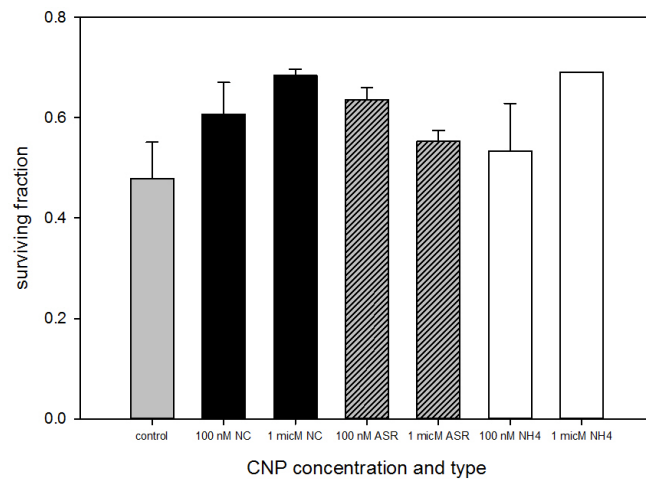


Fig. 4.5 Surviving fraction of A184 non-malignant breast epithelial cells irradiated with an incident energy of 2 MeV protons for a dose of 3.6 Gy vs. CNP concentration and type. An MTT assay was used to assess surviving fraction based on metabolic activity. The control represents the irradiated non-treated cells. Error bars represent standard error.

Fig. 4.5 is a plot of the surviving fraction of cells after treatment with the CNP types ASR, NH4, and NC. This experiment was unintentionally seeded for 250 μ L instead of the usual 200 μ L, adding 20% more cells. This is most likely the reason behind the control being more than double the survival rate as the previous 3.6 Gy experiment and while it makes it difficult to compare survival to other trials, it is sufficient to compare survival between the irradiated control and the

various CNP treated cells due to all the cell counts increasing in each trial. The concentrations and types that displayed the largest increase in cell survival were the 1 μM NC, 100 nM ASR and 1 μM NH₄ with p-values of 0.07, 0.11 and 0.06, respectively. None are less than 0.05, most likely due to the low number of trials (n=4) and could be improved by repeating the experiment and increasing the number trials. It is worth noting that this experiment was run with fresh solution of CNPs and displays higher values for most of the CNP types. Again, age seems to play a factor in the free radical scavenger efficiency as seen in the 1.1 Gy data.

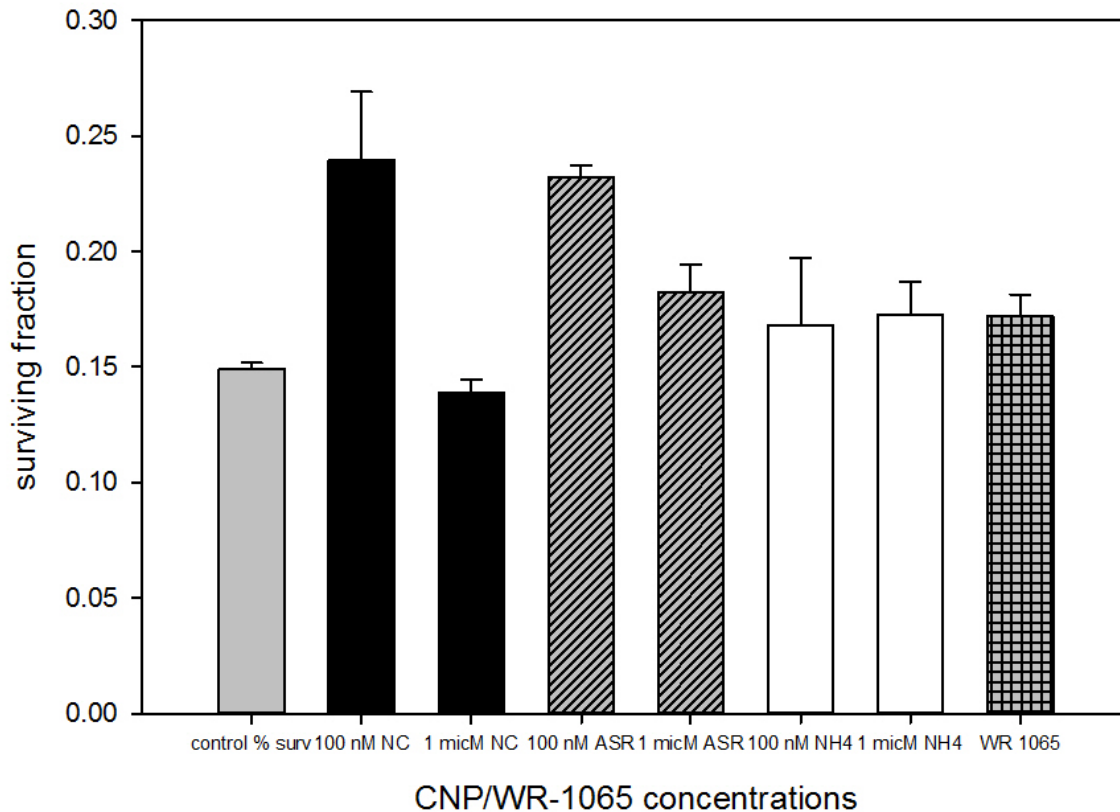


Fig. 4.6 Surviving fraction of A184 non-malignant breast epithelial cells irradiated with an incident energy of 2 MeV protons for a dose of 4.4 Gy vs. CNP concentration and type. An MTT assay was used to assess surviving fraction based on metabolic activity. The control represents the irradiated non-treated cells. WR-1065 treated cell survival is also shown at a 4 mM concentration. Error bars represent standard error.

4 Gy Results

Figure 4.6 shows the surviving fraction of cells when exposed to a dose of 4.4 Gy and include the effects of WR-1065, the active agent in amifostine. Again, the control showed a lower survival rate at a higher dose than the two previous dose measurements. The WR-1065 treated cells indicated a slightly increased survival with a p-value of 0.02 making it statistically significant while the lower concentration of NC and ASR exhibited a 9 and 8 percent increase relative to the control, respectively. However, only the p-value (.004) of the 100 nM ASR concentration was significant. While this research would benefit from more trials to improve the p-values, this plot seems to indicate that all CNP types could be providing some measure of radioprotection to the cells.

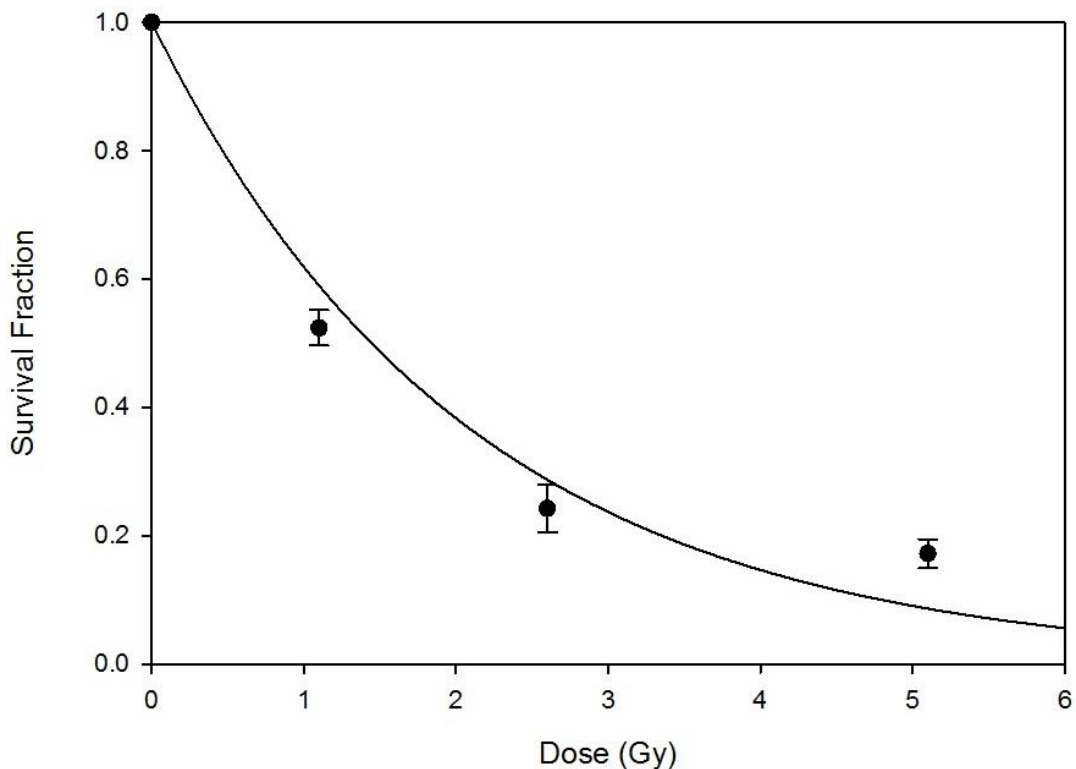


Fig. 4.7 Linear quadratic fit of cell survival curve for A184 non-malignant breast epithelial cells irradiated with an incident energy of 3 MeV protons vs. dose. Cells were assayed using an MTT assay. Error bars represent standard error.

4.3 Survival Curve of 2 MeV and 3 MeV Proton Irradiation

In order to determine if the cell doses were accurate, cell survival values were plotted using the irradiated controls for both the 2 MeV and 3 MeV data and were fitted with the linear quadratic

model, a widely used model for plotting cell survival rates in radiobiology.[89-91, 103, 104] The linear-quadratic model is:

$$\text{Surviving Fraction} = e^{-(\alpha D + \beta D^2)} \quad (4.1)$$

where α and β are constants and D is dose measured in Gy. The 3 MeV survival curve is shown in Fig. 4.7. In the plot, a linear quadratic equation was fitted using the least squares method with an adjusted R^2 value of 0.87. The adjusted R^2 value was used due to the small number of trials ($n=4$) for each data point including the assumed survival fraction of 1 at a dose of 0 Gy. At the 5 Gy dose, the surviving fraction was shown to be higher than expected based on the linear quadratic fit. A possible reason for this could be the MTT assay overestimating cell survival at higher doses due to cells being metabolically active but having little to no proliferation, the true definition of cell survival.[105] An alternative method to account for this overestimation will be discussed later. Also, the cell population is asynchronous and research has shown cells in mitosis and the G_2 (second gap before mitosis) phase have been shown to be more radiosensitive than those in the G_1 (first gap after mitosis) phase or the S phase (DNA synthesis).[106] This can lead to two distinct populations, one more radiosensitive than the other, leading to a survival curve that is initially steep due to high cell kill of the radiosensitive cells, then progressing to a less steep curve at higher doses as the radioresistant population determines survival.[107]

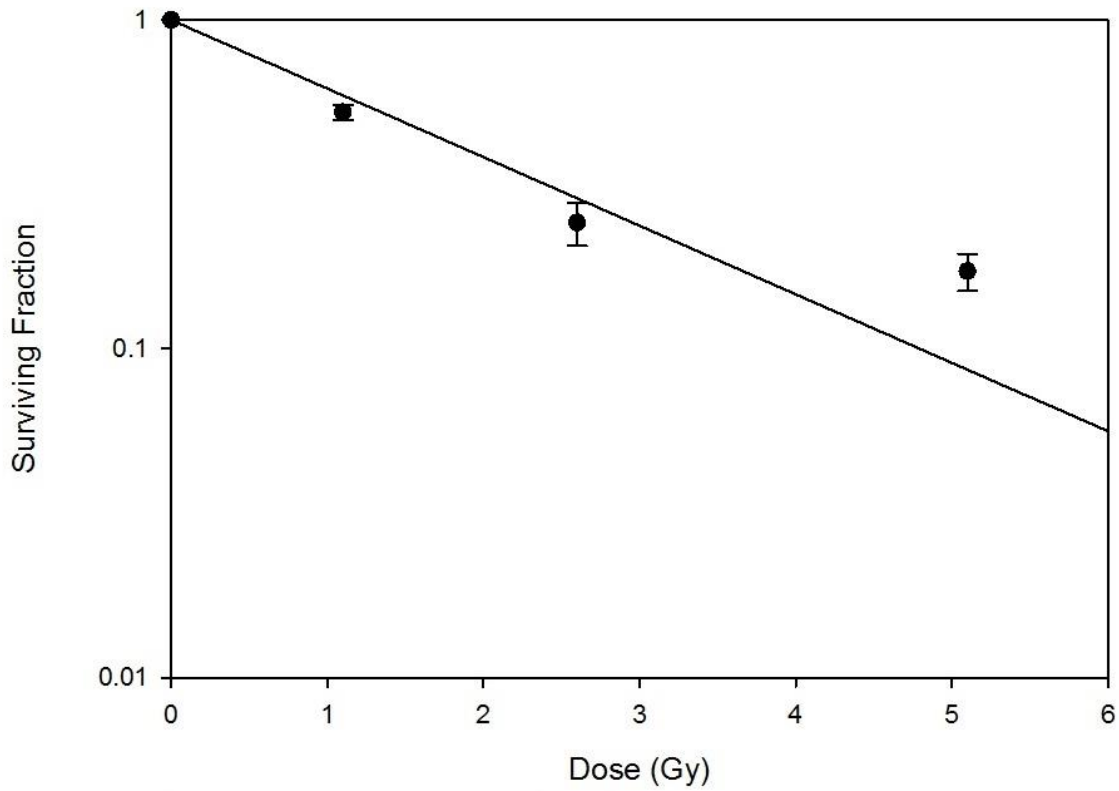


Fig. 4.8 Linear quadratic fit of cell survival curve for A184 non-malignant breast epithelial cells irradiated with an incident energy of 3 MeV protons vs. dose on a semi-logarithmic plot. Cells were assayed using an MTT assay. Error bars represent standard error.

When fitted on a semi-logarithmic plot, as shown in Fig. 4.8, a straight fit is observed with no shoulder which is expected with high LET radiation such as proton radiation as seen in similar experiments. Proton curves from previous research involving hamster cells exhibiting a similar straight fit for a comparable LET value can be found in the literature, indicating somewhat good agreement; however, earlier curves demonstrated a slight shoulder for lower doses, suggesting some repair.[89] This was not present in the survival curves in this research, possibly due to

differences in hamster and human cell morphology, the small sample size for each dose point, or a smaller number of dose values over the same 1-5 Gy range.[108]

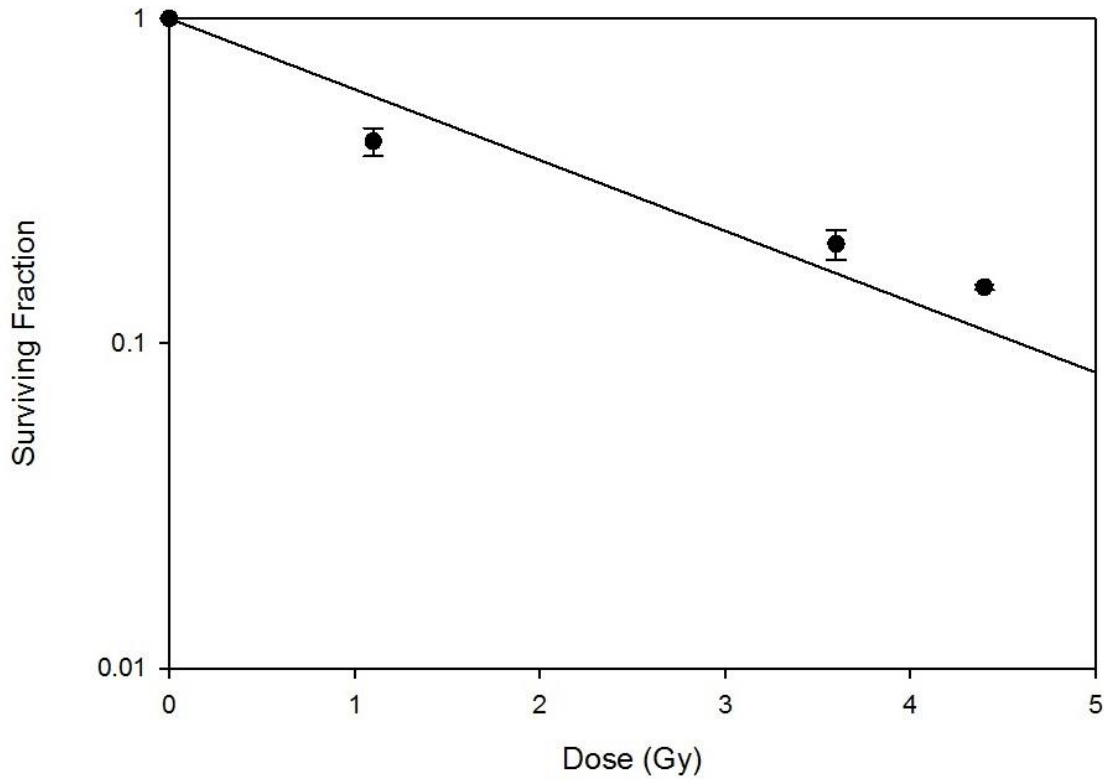


Fig. 4.9 Linear quadratic fit of cell survival curve for A184 non-malignant breast epithelial cells irradiated with an incident energy of 2 MeV protons vs. dose. Cells were assayed using an MTT assay. Error bars represent standard error.

Fig. 4.9 shows the 2 MeV survival curve on a semi-logarithmic plot fit with a linear quadratic equation using the least squares method. The adjusted R^2 value is 0.84 again, due to a small number of trials ($n=4$). As seen at the 4 MeV the lack of shoulder associated with high LET radiation is present and confirms the expected behavior of cell survival decline with

increasing proton radiation dose. While the linear quadratic model is a standard and has remained one in radiobiology, it does not account for DNA repair and transformation of cells after radiation exposure. Transformation could include mutations that allow cells grown in cell cultures to grow beyond the restrictions set when growing cell cultures, finding new ways of survival. Newer models that consider these factors could provide a better fit for high LET radiation that could include a combination of linear, quadratic and higher order terms.[109, 110]

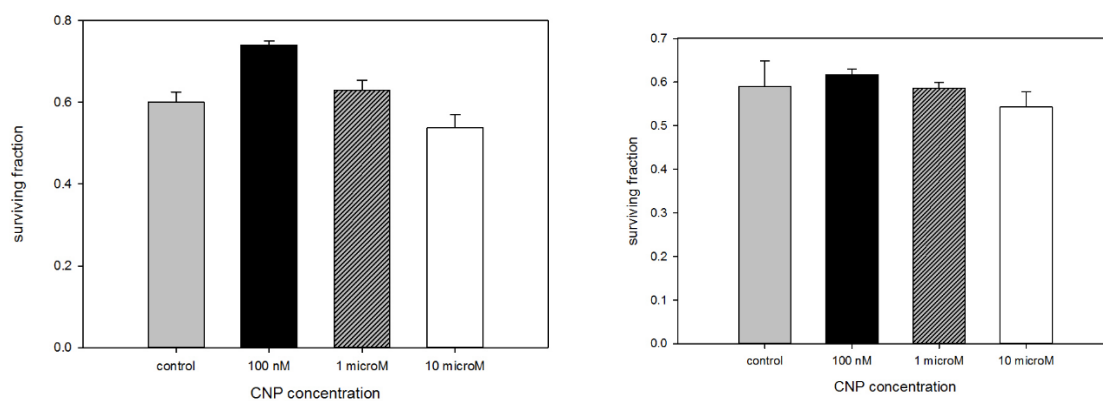


Fig. 4.10a and b. Cell survival vs concentrations for A184 non-malignant breast epithelial cells treated with a dose of 1 Gy at an incident energy of 3 MeV protons. The control represents the non-treated irradiated control. Error bars represent the standard error. The results on the right were taken 7 days after the results on the right.

4.4 3 MeV Proton Irradiation Data

Since the scope of potential research of CNPs and their effect on cells exposed to proton radiation is so broad, different variables were tested in order to find conditions for use in future studies. Many of the plots in this section tested variables such as CNP concentration, time of assay post-irradiation, CNP type and time of exposure to CNPs. In order to determine if concentration of CNPs had an effect on cell survival, cells were exposed to concentrations of 100

nM, 1 μ M, and 10 μ M and the results were measured at a dose of 1 Gy. The results are shown in Fig. 4.10. While both plots displayed a decrease in cell survival as the CNP concentration increases, Fig. 4.10a indicated a greater cell survival rate and the 100 nM and had a calculated p-value of 0.01 indicating a statistical significance. While a trend can be seen showing there is a higher cell survival at 100 nM concentration, more data is needed to come to a definitive conclusion on the efficacy of the CNPs at the 3 MeV proton energy.

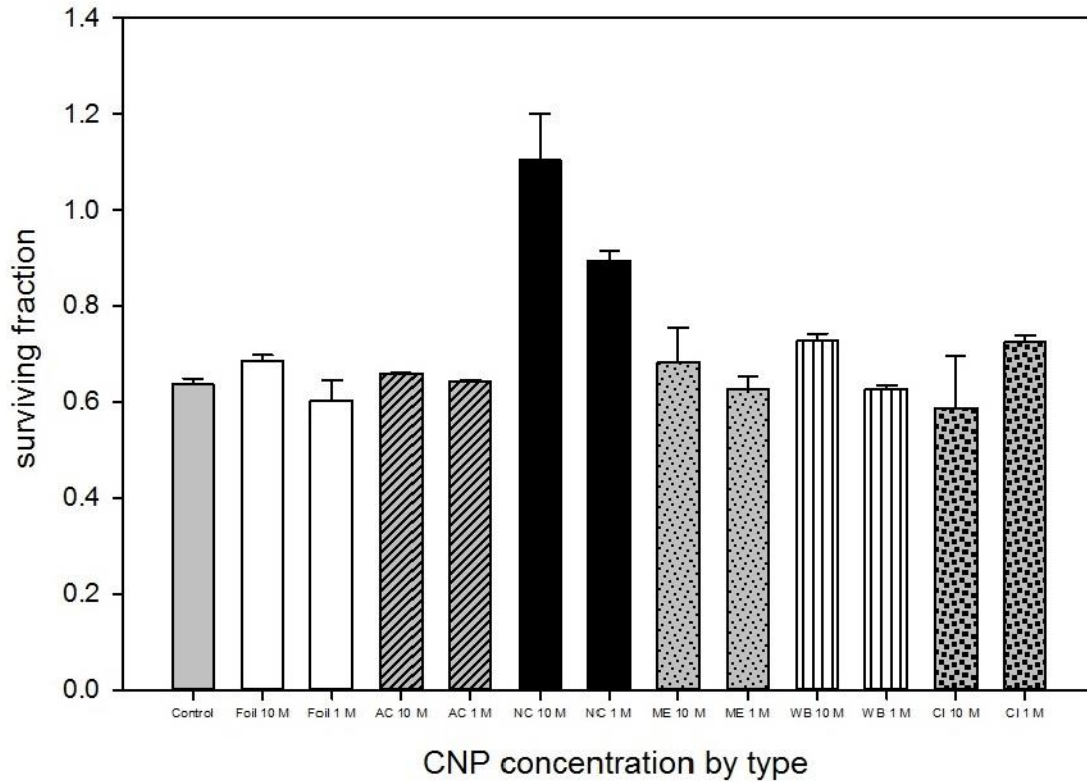


Fig. 4.11 Cell survival fractions for various CNP types at 10 μ M and 1 μ M concentrations for A184 non-malignant breast epithelial cells treated with an incident energy of 3 MeV protons at a dose of 1 Gy. NC shows values higher than 1 due to contamination of the CNPs when they were produced. Error bars represent standard error.

CNP type offers a wide variety of potential radioprotectors to be tested and for this project, many were tested at various concentrations. Various CNPs types were tested at 3 MeV in the same manner the others were at the 3 MeV proton energy and the results are shown in Fig. 4.11. The CNP types were labeled according the names attached to the vials or whatever distinguishing factor existed on the vial as in the case of the “foil” CNP type. In the case of all the CNP varieties measured for this experiment, nothing showed a significant increase in cell survival. In addition, the NC CNPs were found to be contaminated by a misstep in the synthesis process but was unknown until survival fractions were found to be higher than one The NC CNPs were cultured and they were found to contain bacteria. From that point, all CNP solutions were tested for contamination upon arrival before being used to treat the cells.

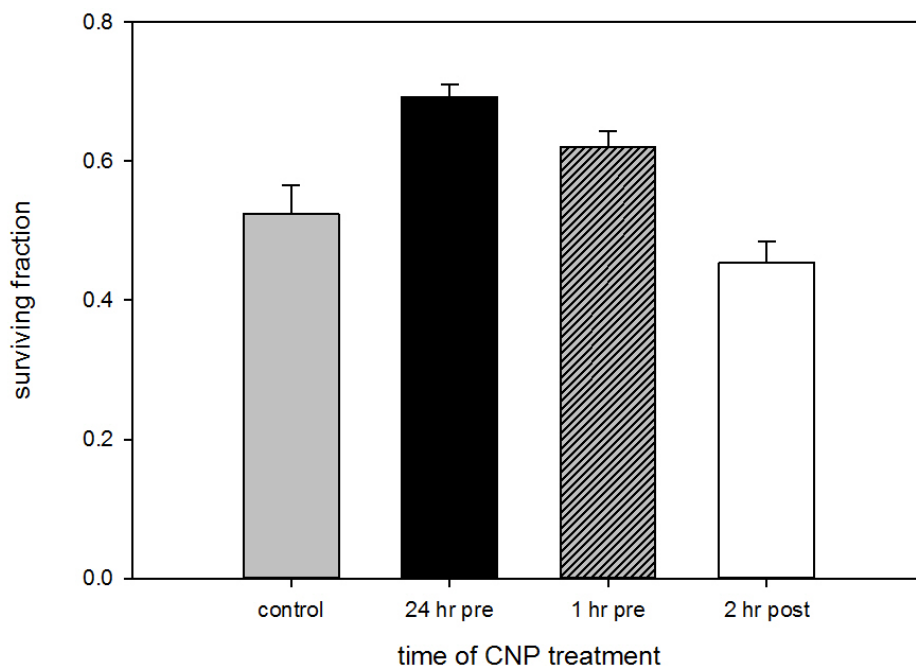


Fig. 4.12 Surviving fraction vs. time of CNP treatment for A184 non-malignant epithelial breast cells treated with 100 nM CNP treatment and irradiated with protons at an incident energy of 3 MeV for a dose of 1 Gy. Treatments took place 24 hours and 1 hour pre-irradiation and 2 hours post-irradiation. Error bars represent standard error.

The time of application of the CNPs was of interest since a practical application in the future could require an administration of the CNPs in the event of an unexpected radiation exposure event. The question was asked would the CNPs be effective in providing radiation protection if applied immediately before or after proton irradiation of the cells. For the other experiments, the standard exposure time of the cells to the CNPs was 24 hours. To test the time of exposure, the cells were treated either 1 hour pre-irradiation or 2 hours post irradiation. The results are shown in Fig. 4.12. The 24 hour pre-irradiation clearly allowed for the CNPs to increase cell protection compared to the irradiated control and is confirmed with a p-value of 0.02 giving statistical significance to this increase in survival. While the 1 hour pre-irradiation application to the cells is not as effective as the 24 hour exposure, there is higher cell survival than the irradiated control as well but has a p-value of .10. The post irradiation application demonstrates that treating cells after irradiation is not effective in increasing cell survival.

Another time dependent variable that was tested was the time of the MTT assay once the cell were irradiated. The standard assay time for all the experiments performed was 24 hours post irradiation but for this experiment, the 24 hour assay was compared to the 48 hour assay. The results are shown in Fig 4.13. The time of application was at 24 hours pre, 1 hour pre-irradiation and 2 hours post-irradiation. The CNP concentration was 100 nM.

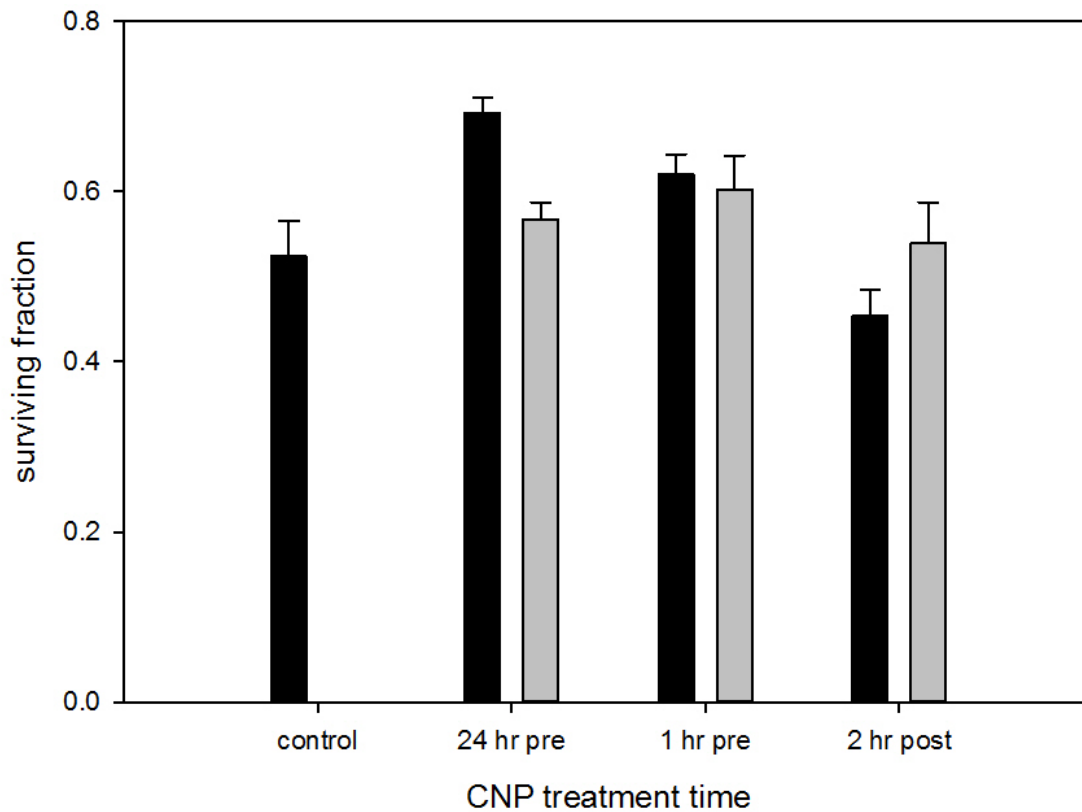


Fig. 4.13 Surviving fraction vs. CNP treatment time and assay time for A184 non-malignant breast epithelial cells irradiated with protons at an incident energy of 3 MeV for a dose of 1 Gy. The black represents the 24 hour assay while the gray represents the 48 hour assay. The control assay was performed at 24 hours. The error bars represent standard error.

The pretreated cells showed lower cell survival after 48 hours, possibly due to a cell cycle time greater than 24 hours allowing for the cells to progress through a mitosis that caused them to die upon reproduction (apoptosis). The p-value for the 24 vs. 48 hour assay for the 24 hour pre-treatment was .003 showing definite decrease in cell metabolic activity. Previous research on

cells similar to the A184 cell line show a cell cycle time that ranges from 24-28 hours.[111, 112] The 2 hour post treatment showed a higher cell survival possibly due to the fact that a longer time between irradiation and the assay allows for more time for cell repair. However, with a p-value of 0.19, it is not statistically significant.

4.5 TUNEL Assay Data

The TUNEL assay allowed for the imaging of the cell nuclei and provides an indicator of the DNA strand nicks that are caused by radiation exposure. The DAPI that was used to stain the cells is a marker for DNA and has a blue fluorescence. The TUNEL fluorophore that labels the DNA nick ends exhibits a red fluorescence. The images are shown in Fig. 4.15 and 4.16. The TUNEL images show that the irradiated controls contain more of the TUNEL marker indicating more DNA damage than those treated with the NH4 and ASR CNPs. All were treated at 2 MeV incident proton energy for a dose of 2.8 Gy. In addition, there are more cells present on the plates containing the CNPs than in those that were irradiated without CNP treatment. This suggests that while the cells in the treated wells may have been damaged, they were able to survive, repairing and continuing to multiply unlike those that were not treated which led to cell death and detachment from the plate. This could be tested with assays that specifically measure DNA repair and the factors that influence DNA repair to determine if they are more abundant in CNP treated cells than in the non-treated cells. The TUNEL images show that the CNPs have a potential to be a radioprotector for cells exposed to charged particle radiation. A clustering effect also is shown in both figures although it is unknown if it affects survival.

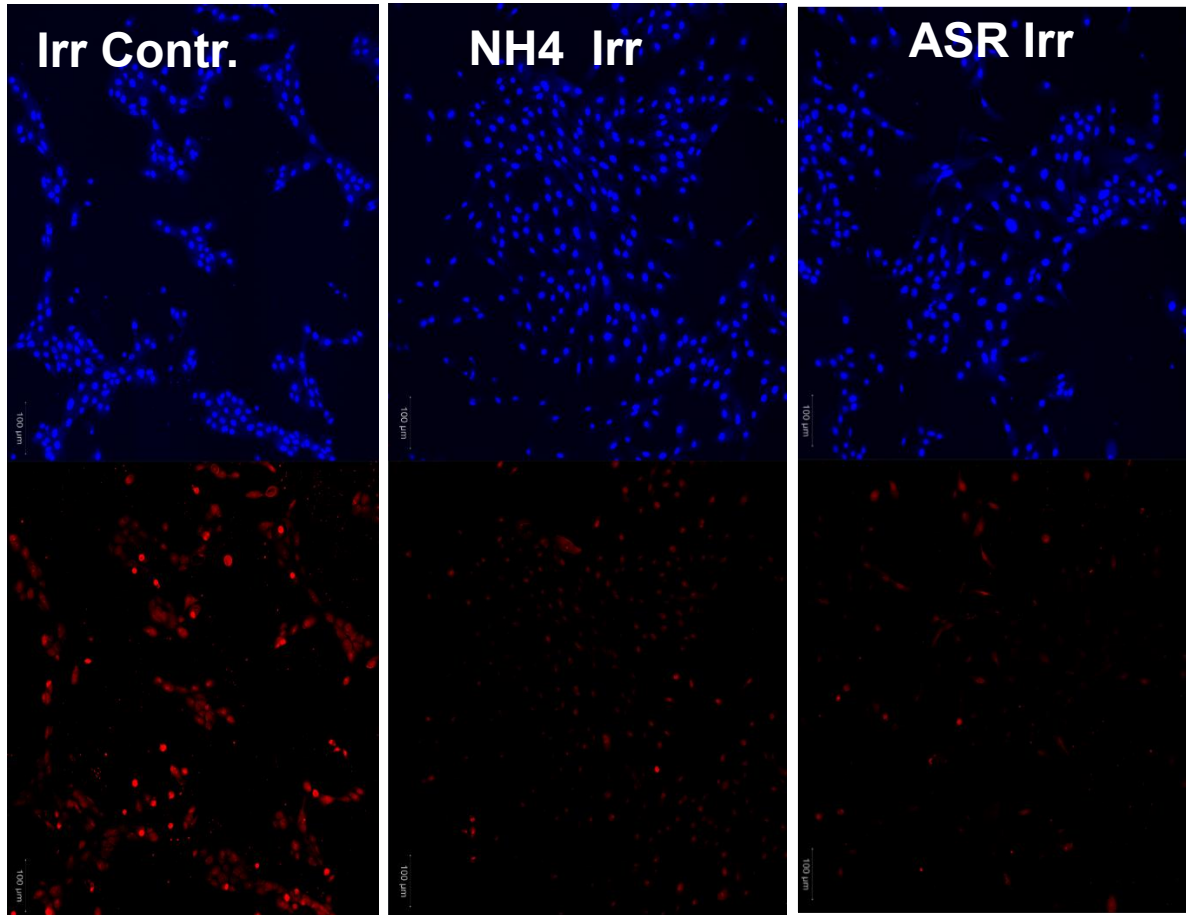


Fig. 4.14 TUNEL images showing DNA damage (red) and DNA (blue). A184 non-malignant breast epithelial cells were irradiated for a dose of 2.8 Gy at an incident proton energy of 2 MeV. The image on the left was an irradiated control while the two on the right were the CNP treated cells. The irradiated control shows brighter TUNEL markers revealing more damage than CNP treated cells.

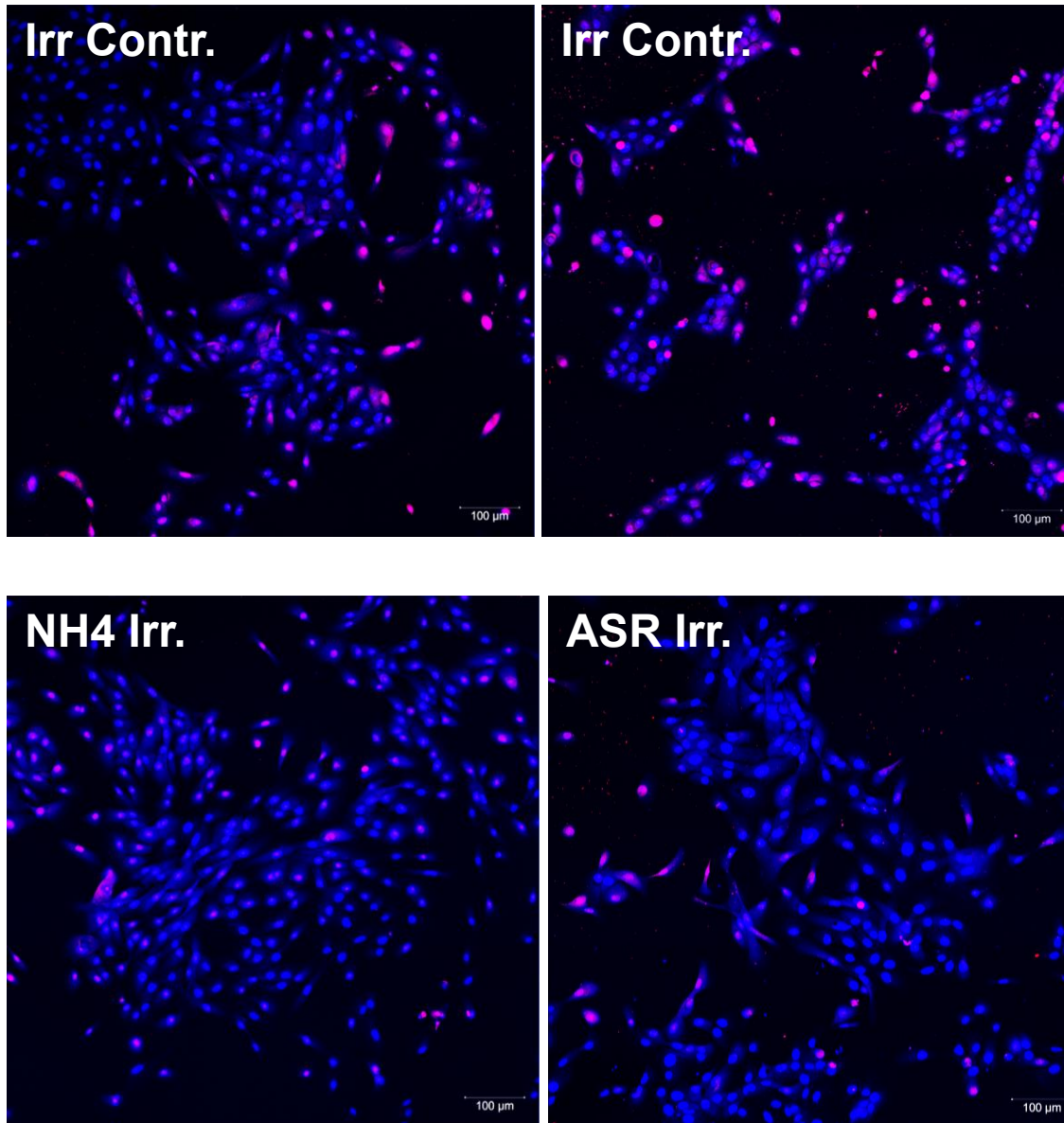


Fig. 4.15 A184 non-malignant breast epithelial cells were irradiated for a dose of 2.8 Gy at an incident proton energy of 2 MeV. The top two images are the irradiated controls and the bottom images are the CNP treated cells. TUNEL images are merged with both the DAPI (blue) and the TUNEL fluorophore (red) to show evidence of the DNA and where it is damaged.

Chapter 5: Discussion

The aims of this research were 1) to develop a system with which A184 breast epithelial breast cells could be irradiated with protons to a specified dose, 2) to determine the efficacy of CNPs as a viable radioprotector for normal cells and to test different variables to determine cell survival as well as develop a cell survival curve to confirm a consistent dose delivery system at different energies and 3) to perform a DNA damage assay to determine the damage to CNP treated cells.

5.1 Radiation Beam Dose Measurement System

The measured beam current and published stopping powers were used to determine dose to the cells, a process that has proved to be effective and outlined in detail in the literature.[113] While this method is based on averaged quantities including LET and mass stopping powers, it was effective for this research considering the focus was the effect of relative dose to cells with and without CNP treatment rather than absolute dose.

The uncertainty in relative dose is estimated to be less than 10%. This is due to fluctuations in the beam current and control of the exposure times. The YAG crystals used were useful in determining the variation across the flux incident on the cells and allowed for a more uniform dose across the entire surface area of the cells. While they were sufficient to collect preliminary data in this new area of radiation biology research, a more advanced beam imaging system would be advantageous in the future to allow for a more streamlined process to characterize the beam. A method of determining dose would be advantageous in seeing the effect that CNPs have at different absolute doses. The use of surface barrier detectors or an ionization

chamber would be a valid method of measuring both the flux and the energy spread at the cell plate's position in the path of the beam.

While the titanium foil allowed for a reduction in proton beam energy loss while maintaining vacuum, stronger metal alloy foils could allow for a thinner exit window and a further reduction of energy loss can be obtained, including Havar foil which has been used in other research experiments.[114] With a thinner window, it could be possible to test lower proton energies to test the CNP effect at higher LET values.

5.2 Cell Survival Data

Due to the immensely wide scope of the emerging field of nanoparticle research particularly in the area of charged-particle radiation, there were so many potential areas of study that they had to be narrowed down to a few variables of interest due to availability of resources. Cell survival curves were measured first to ensure the dose administered was within range of what was expected based on earlier proton radiation research as detailed earlier. Using the 2 MeV and 3 MeV incident proton energy beams, the survival curves proved to have good agreement with regards to direct relationship: as dose was increased, cell kill also increased and could be plotted with limited success with the linear quadratic model. The shoulder present on proton radiation survival curves in earlier research was not seen in this research and may require more dose trials at smaller intervals to obtain a more accurate dose curve. However, as mentioned previously, the proton radiation cell survival curve could be unique when treating human cells as opposed to treating hamster cells which were the focus in earlier studies. Also, at higher doses, radiation resistant populations were shown to survive which could be caused due to an overestimation by the MTT assay for cell survival as discussed earlier. In addition, due to the

asynchronous cell cycle of the cell culture, the combination of radiosensitive and radioresistant cells causes an initial steep dose response that becomes less steep at higher doses.

Once proton radiation was shown to be effective with cell irradiation, the various types of CNPs were tested to determine if they had the same efficacy of radioprotection as they do with regards to x-rays. While the CNPs did show promise in increasing cell metabolic activity as compared to cells that were not treated, the data suggests that it is not conclusive. Part of the issue could be due to the plating process of cells in the individual wells, while the magnitude of the number of cells can be determined and controlled to be consistent from well to well, cell growth, much like radiation, is a stochastic process. The variation would require an assay that counts cells individually that are still proliferating, the true definition of a living cell. A clonogenic assay is a good example of one that could perform this function. Also, while MTT assays are useful in determining metabolic activity of the cells at the moment they are assayed, it may not account for cells that may be metabolically active but can no longer proliferate, giving a false fraction of survival, especially at higher doses. In addition, while the assays were performed at 24 hours after irradiation of the cells, it may require a longer time for the cells to become active once cell repair is finished, or to go through a cell cycle to perform apoptosis, therefore a 48 hour or 72 hour wait time may allow for repair and a restart of the cell cycle or apoptosis.

The cell concentration showed no definitive value where cell protection is peaked, however, 100 nM showed promise in different trials. While higher concentrations showed potential, it may not be feasible in a clinical setting due to complication with high concentrations of metal in the blood possibly causing clots in the circulatory system. Therefore, it is necessary

to test lower concentrations and test in smaller intervals both above and below 100 nM to determine if it is truly the ideal concentration.

The main method of CNP radioprotection has been shown to be free radical scavenging which is abundant with indirect radiation damage caused by x-rays, which is the main reason for a much higher cell survival rate with previous research. Charged particle radiation is responsible for more direct damage to the DNA with less indirect damage to the DNA from free radicals. This could be the reason why the CNPs were not as effective in maintaining metabolic activity as it was with cell exposure to x-rays.

Since conducting this experiment, new research suggested that time plays a factor in the effectiveness of the CNPs to scavenge free radicals. In a recent study, CNPs had showed reduced scavenging with different solutions aged 1,7, 14 and 28 days, even assisting the radicals rather than inhibiting them after 28 days.[102] The change is believed to be due to the agglomeration of the CNPs as time progresses, reducing the effective surface area and consequently the oxygen vacancies present on the surface of the nanoparticles, hindering the mechanism the CNPs use to scavenge the free radicals. Similar studies confirm these findings showing that upon aging, the Ce^{+3} transition to Ce^{+4} reducing the active sites for free radical scavenging. A higher $\text{Ce}^{+3}/\text{Ce}^{+4}$ has been shown to correlate with higher oxygen and electron vacancies and a smaller size, increasing the surface area/volume ratio.[115] A higher initial concentration of Ce^{+3} is required for redox cycling as well as activity in the biological media.[116]

5.3 DNA Damage Assay

The most promising results from this research were presented by the TUNEL assay which gives a visual representation of the DNA damage to treated and untreated cells. Unlike the MTT assay, this allows for a direct determination of the effect of the proton radiation on the DNA. Since proton radiation provides direct damage, interacting directly with the DNA strands and causing single and double strand breaks that may lead to apoptotic cell death, the irradiated cells that were not treated showed widespread damage and lower confluence possibly due to many cells dying between irradiation and the assay procedure. The results of the TUNL assay convey a radioprotection aspect of the CNPs that were seen in earlier research with x-rays.[17]

5.4 Future Directions

As mentioned before, the scope of this new field of radiation research is broad and extends over many different areas. While the research here seems to point to a radioprotector that is possibly as effective as amifostine, its potential as a radiosensitizer is very promising as seen in the literature.[54, 68, 69] All research so far in regards to radiosensitizers has been measuring the effect to cancer cells exposed to x-rays but no experimental data has been published showing results with charged particle radiation. Also, there is an extensive amount of nanoparticle types that have shown promising results in the area of radiation therapy including gold, platinum and gadolinium.[117-122] With the capabilities of the ECU Pelletron Accelerator, different ions can be tested as well to determine efficacy against heavy charged particles. With the rapidly emerging field of heavy ion therapy, it would be valuable to test the effects of different nanoparticles used to treat tumor cells, possibly increasing cell killing while protecting normal

cells. If the benefits of CNPs could have a two-fold benefit as a radioprotector and radiosensitizer for normal cells and tumor cells respectively, it would be valuable in radiation cancer therapy. If the *in vitro* studies show promise for data for the protection and sensitization, then the next step would be *in vivo* studies with mice. For proton and heavy ion therapy, a higher beam energy would be necessary for mouse models and would require a larger accelerator facility than is currently at ECU. As more potentially effective nanoparticles are discovered, many new avenues of research in the area of radiation protection and sensitization should emerge.

References

1. Mettler Jr, F.A., B.R. Thomadsen, M. Bhargavan, D.B. Gilley, J.E. Gray, J.A. Lipoti, J. McCrohan, T.T. Yoshizumi, and M. Mahesh, *Medical radiation exposure in the US in 2006: preliminary results*. Health physics, 2008. **95**(5): p. 502-507.
2. *Doses Our Daily Lives*. October 2014; Available from: www.nrc.gov/about-nrc/radiation/around-us/doses-daily-lives.html.
3. Hellweg, C.E. and C. Baumstark-Khan, *Getting ready for the manned mission to Mars: the astronauts' risk from space radiation*. Naturwissenschaften, 2007. **94**(7): p. 517-526.
4. Hosseinimehr, S.J., *Trends in the development of radioprotective agents*. Drug discovery today, 2007. **12**(19): p. 794-805.
5. Khan, F.M. and J.P. Gibbons, *Khan's the Physics of Radiation Therapy* 2014: Lippincott Williams & Wilkins.
6. Cucinotta, F.A., *Space Radiation Cancer Risks*. 2007.
7. Attix, F.H., *Introduction to radiological physics and radiation dosimetry* 2008: John Wiley & Sons.
8. Saw, C.B., *Foundation of radiological physics* 2004: CB Saw Pub.
9. Turner, J.E. and C.A. Kelsey, *Atoms, radiation, and radiation protection* 1995: Wiley New York.
10. Podgorsak, E.B., *Review of radiation oncology physics: a handbook for teachers and students*. Vienna, International Atomic Energy Agency. Educational reports series, 2003.
11. Carron, N.J., *An introduction to the passage of energetic particles through matter* 2006: CRC Press.
12. Halperin, E.C., L.W. Brady, D.E. Wazer, and C.A. Perez, *Perez & Brady's Principles and Practice of Radiation Oncology* 2013: Lippincott Williams & Wilkins.
13. Sherer, M.A.S., P.J. Visconti, E.R. Ritenour, and K. Haynes, *Radiation protection in medical radiography* 2014: Elsevier Health Sciences.
14. Nikjoo, H., S. Uehara, and D. Emfietzoglou, *Interaction of radiation with matter* 2012: CRC Press.
15. Raviraj, J., V.K. Bokkasam, V.S. Kumar, U.S. Reddy, and V. Suman, *Radiosensitizers, radioprotectors, and radiation mitigators*. Indian Journal of Dental Research, 2014. **25**(1): p. 83.
16. Cohen-Jonathan, E., E.J. Bernhard, and W.G. McKenna, *How does radiation kill cells? Current opinion in chemical biology*, 1999. **3**(1): p. 77-83.
17. Tarnuzzer, R.W., J. Colon, S. Patil, and S. Seal, *Vacancy engineered ceria nanostructures for protection from radiation-induced cellular damage*. Nano letters, 2005. **5**(12): p. 2573-2577.
18. Brizel, D.M., T.H. Wasserman, M. Henke, V. Strnad, V. Rudat, A. Monnier, F. Eschwege, J. Zhang, L. Russell, and W. Oster, *Phase III randomized trial of amifostine as a radioprotector in head and neck cancer*. Journal of Clinical Oncology, 2000. **18**(19): p. 3339-3345.

19. Sattler, J.A., *Comparison of Two Human Cell Lines Following Exposure to Low Dose Radiation and Treatment with Soybean Miso and its active ingredient Genistein*, in *Department of Physics* 2013, East Carolina University
20. Colon, J., L. Herrera, J. Smith, S. Patil, C. Komanski, P. Kupelian, S. Seal, D.W. Jenkins, and C.H. Baker, *Protection from radiation-induced pneumonitis using cerium oxide nanoparticles*. *Nanomedicine: Nanotechnology, Biology and Medicine*, 2009. **5**(2): p. 225-231.
21. Ziegler, J.F., M. Ziegler, and J. Biersack, *SRIM—The stopping and range of ions in matter (2010)*. *Nuclear Instruments and Methods in Physics Research Section B: Beam Interactions with Materials and Atoms*, 2010. **268**(11): p. 1818-1823.
22. Hall, E.J. and A.J. Giaccia, *Radiobiology for the Radiologist* 2006: Wolters Kluwer Health.
23. HANAI M. YAZU K. HIEDA, R., *On the experimental distinction between ssbs and dsbs in circular DNA*. *International journal of radiation biology*, 1998. **73**(5): p. 475-479.
24. Cassatt, D.R., C.A. Fazenbaker, C.M. Bachy, and M.S. Hanson. *Preclinical modeling of improved amifostine (Ethyol) use in radiation therapy*. in *Seminars in Radiation Oncology*. 2002. Elsevier.
25. Dziegielewski, J., J.E. Baulch, W. Goetz, M.C. Coleman, D.R. Spitz, J.S. Murley, D.J. Grdina, and W.F. Morgan, *WR-1065, the active metabolite of amifostine, mitigates radiation-induced delayed genomic instability*. *Free Radical Biology and Medicine*, 2008. **45**(12): p. 1674-1681.
26. Khodarev, N.N., Y. Kataoka, J.S. Murley, R.R. Weichselbaum, and D.J. Grdina, *Interaction of amifostine and ionizing radiation on transcriptional patterns of apoptotic genes expressed in human microvascular endothelial cells (HMEC)*. *International Journal of Radiation Oncology* Biology* Physics*, 2004. **60**(2): p. 553-563.
27. DeNeve, W.J., C.K. Everett, J.E. Suminski, and F.A. Valeriote, *Influence of WR2721 on DNA cross-linking by nitrogen mustard in normal mouse bone marrow and leukemia cells in vivo*. *Cancer research*, 1988. **48**(21): p. 6002-6005.
28. Johnke, R.M., Sattler, Jennifer A., Allison, Ron R., *Radioprotective agents for radiation therapy: future trends*. *Future Oncology*, 2014. **10**(15): p. 2345-57.
29. Millar, J., T. McElwain, R. Clutterbuck, and E. Wist, *The modification of melphalan toxicity in tumor bearing mice by s-2-(3-aminopropylamino)-ethylphosphorothioic acid (WR2721)*. *American journal of clinical oncology*, 1982. **5**(3): p. 321-328.
30. *MEDIndia Amifostine Pricelist*. 2014; <http://www.medindia.net/drug-price/amifostine.htm>;
31. Mitchell, J.B., W. DeGraff, D. Kaufman, M.C. Krishna, A. Samuni, E. Finkelstein, M.S. Ahn, S.M. Hahn, J. Gamson, and A. Russo, *Inhibition of oxygen-dependent radiation-induced damage by the nitroxide superoxide dismutase mimic, tempol*. *Archives of biochemistry and biophysics*, 1991. **289**(1): p. 62-70.
32. Hahn, S.M., Z. Tochner, C.M. Krishna, J. Glass, L. Wilson, A. Samuni, M. Sprague, D. Venzon, E. Glatstein, and J.B. Mitchell, *Tempol, a stable free radical, is a novel murine radiation protector*. *Cancer research*, 1992. **52**(7): p. 1750-1753.
33. Martin, R., S. Broadhurst, S. D'Abrew, R. Budd, R. Sephton, M. Reum, and D. Kelly, *Radioprotection by DNA ligands*. *The British journal of cancer. Supplement*, 1996. **27**: p. S99.

34. Tawar, U., S. Bansal, S. Shrimal, M. Singh, and V. Tandon, *Nuclear condensation and free radical scavenging: a dual mechanism of bisbenzimidazoles to modulate radiation damage to DNA*. Molecular and cellular biochemistry, 2007. **305**(1-2): p. 221-233.
35. Singh, V.K. and V.S. Yadav, *Role of cytokines and growth factors in radioprotection*. Experimental and molecular pathology, 2005. **78**(2): p. 156-169.
36. Maisin, J., *Bacq and Alexander award lecture chemical radioprotection: past, present and future prospects*. International journal of radiation biology, 1998. **73**(4): p. 443-450.
37. Felemovicius, I., M.E. Bonsack, M.L. Baptista, and J.P. Delaney, *Intestinal radioprotection by vitamin E (alpha-tocopherol)*. Annals of surgery, 1995. **222**(4): p. 504.
38. Kumar, K.S., V. Srinivasan, R. Toles, L. Jobe, and T.M. Seed, *Nutritional approaches to radioprotection: Vitamin E*. Military medicine, 2002. **167**(2 Suppl): p. 57-59.
39. Keithahn, C. and A. Lerchl, *5-Hydroxytryptophan is a more potent in vitro hydroxyl radical scavenger than melatonin or vitamin C*. Journal of pineal research, 2005. **38**(1): p. 62-66.
40. Lusardi, P., E. Piazza, and R. Fogari, *Cardiovascular effects of melatonin in hypertensive patients well controlled by nifedipine: a 24-hour study*. British journal of clinical pharmacology, 2000. **49**(5): p. 423-427.
41. Kitts, D.D., A.N. Wijewickreme, and C. Hu, *Antioxidant properties of a North American ginseng extract*. Molecular and cellular biochemistry, 2000. **203**(1-2): p. 1-10.
42. Attele, A.S., J.A. Wu, and C.-S. Yuan, *Ginseng pharmacology: multiple constituents and multiple actions*. Biochemical pharmacology, 1999. **58**(11): p. 1685-1693.
43. Lee, T.-K., R.M. Johnke, R.R. Allison, K.F. O'Brien, and L.J. Dobbs, *Radioprotective potential of ginseng*. Mutagenesis, 2005. **20**(4): p. 237-243.
44. Lee, T.-K., R.R. Allison, K.F. O'Brien, P.G. Khazanie, R.M. Johnke, R. Brown, R.M. Bloch, M.L. Tate, L.J. Dobbs, and P.J. Kragel, *Ginseng reduces the micronuclei yield in lymphocytes after irradiation*. Mutation Research/Genetic Toxicology and Environmental Mutagenesis, 2004. **557**(1): p. 75-84.
45. Henkel, J., *Soy. Health claims for soy protein, questions about other components*. FDA consumer, 2000. **34**(3): p. 13.
46. Greendale, G.A., G. FitzGerald, M.-H. Huang, B. Sternfeld, E. Gold, T. Seeman, S. Sherman, and M. Sowers, *Dietary soy isoflavones and bone mineral density: results from the study of women's health across the nation*. American journal of epidemiology, 2002. **155**(8): p. 746-754.
47. Huang, H.-Y., H.-P. Yang, H.-T. Yang, T.-C. Yang, M.-J. Shieh, and S.-Y. Huang, *One-year soy isoflavone supplementation prevents early postmenopausal bone loss but without a dose-dependent effect*. The Journal of nutritional biochemistry, 2006. **17**(8): p. 509-517.
48. Goldwyn, S., A. Lazinsky, and H. Wei, *Promotion of health by soy isoflavones: efficacy, benefit and safety concerns*. Drug metabolism and drug interactions, 2000. **17**(1-4): p. 261-290.
49. Landauer, M.R., V. Srinivasan, and T.M. Seed, *Genistein treatment protects mice from ionizing radiation injury*. Journal of Applied Toxicology, 2003. **23**(6): p. 379-385.

50. Yashar, C.M., W.J. Spanos, D.D. Taylor, and C. Gercel-Taylor, *Potential of the radiation effect with genistein in cervical cancer cells*. *Gynecologic oncology*, 2005. **99**(1): p. 199-205.
51. Rucinska, A., M. Roszczyk, and T. Gabryelak, *Cytotoxicity of the isoflavone genistein in NIH 3T3 cells*. *Cell biology international*, 2008. **32**(8): p. 1019-1023.
52. Hsieh, C.-Y., R.C. Santell, S.Z. Haslam, and W.G. Helferich, *Estrogenic effects of genistein on the growth of estrogen receptor-positive human breast cancer (MCF-7) cells in vitro and in vivo*. *Cancer research*, 1998. **58**(17): p. 3833-3838.
53. Salata, O.V., *Applications of nanoparticles in biology and medicine*. *Journal of nanobiotechnology*, 2004. **2**(1): p. 3.
54. Das, S., J.M. Dowding, K.E. Klump, J.F. McGinnis, W. Self, and S. Seal, *Cerium oxide nanoparticles: applications and prospects in nanomedicine*. *Nanomedicine*, 2013. **8**(9): p. 1483-1508.
55. Karakoti, A., N. Monteiro-Riviere, R. Aggarwal, J. Davis, R. Narayan, W. Self, J. McGinnis, and S. Seal, *Nanoceria as antioxidant: synthesis and biomedical applications*. *Jom*, 2008. **60**(3): p. 33-37.
56. Heckert, E.G., A.S. Karakoti, S. Seal, and W.T. Self, *The role of cerium redox state in the SOD mimetic activity of nanoceria*. *Biomaterials*, 2008. **29**(18): p. 2705-2709.
57. Jessica, E., *Nanoceria exhibit redox state-dependent catalase mimetic activity*. *Chemical Communications*, 2010. **46**(16): p. 2736-2738.
58. Karakoti, A.S., S. Singh, A. Kumar, M. Malinska, S.V. Kuchibhatla, K. Wozniak, W.T. Self, and S. Seal, *PEGylated nanoceria as radical scavenger with tunable redox chemistry*. *Journal of the American Chemical Society*, 2009. **131**(40): p. 14144-14145.
59. Dowding, J.M., T. Dosani, A. Kumar, S. Seal, and W.T. Self, *Cerium oxide nanoparticles scavenge nitric oxide radical (NO)*. *Chemical Communications*, 2012. **48**(40): p. 4896-4898.
60. Xue, Y., Q. Luan, D. Yang, X. Yao, and K. Zhou, *Direct evidence for hydroxyl radical scavenging activity of cerium oxide nanoparticles*. *The Journal of Physical Chemistry C*, 2011. **115**(11): p. 4433-4438.
61. Asati, A., S. Santra, C. Kaittanis, S. Nath, and J.M. Perez, *Oxidase-Like Activity of Polymer-Coated Cerium Oxide Nanoparticles*. *Angewandte Chemie International Edition*, 2009. **48**(13): p. 2308-2312.
62. Colon, J., N. Hsieh, A. Ferguson, P. Kupelian, S. Seal, D.W. Jenkins, and C.H. Baker, *Cerium oxide nanoparticles protect gastrointestinal epithelium from radiation-induced damage by reduction of reactive oxygen species and upregulation of superoxide dismutase 2*. *Nanomedicine: Nanotechnology, Biology and Medicine*, 2010. **6**(5): p. 698-705.
63. Mamotyuk, E., V. Klochkov, G. Grygorova, S. Yefimova, and Y.V. Malyukin, *Radioprotective Effect of CeO₂ and GdEuVO₄ Nanoparticles in "In Vivo" Experiments*, in *Nanoscience Advances in CBRN Agents Detection, Information and Energy Security* 2015, Springer. p. 193-197.
64. Lin, W., Y.-w. Huang, X.-D. Zhou, and Y. Ma, *Toxicity of cerium oxide nanoparticles in human lung cancer cells*. *International Journal of Toxicology*, 2006. **25**(6): p. 451-457.
65. Alili, L., M. Sack, A.S. Karakoti, S. Teuber, K. Puschmann, S.M. Hirst, C.M. Reilly, K. Zanger, W. Stahl, and S. Das, *Combined cytotoxic and anti-invasive properties of redox-*

- active nanoparticles in tumor–stroma interactions*. *Biomaterials*, 2011. **32**(11): p. 2918-2929.
66. Ibañez, I.L., C. Notcovich, P.N. Catalano, M.G. Bellino, and H. Durán, *The redox-active nanomaterial toolbox for cancer therapy*. *Cancer letters*, 2015.
 67. Sayin, V.I., M.X. Ibrahim, E. Larsson, J.A. Nilsson, P. Lindahl, and M.O. Bergh, *Antioxidants Accelerate Lung Cancer Progression in Mice*. *Science Translational Medicine*, 2014. **6**(221): p. 221ra15.
 68. Madero-Visbal, R.A., B.E. Alvarado, J.F. Colon, C.H. Baker, M.S. Wason, B. Isley, S. Seal, C.M. Lee, S. Das, and R. Mañon, *Harnessing nanoparticles to improve toxicity after head and neck radiation*. *Nanomedicine: Nanotechnology, Biology and Medicine*, 2012. **8**(7): p. 1223-1231.
 69. Wason, M.S., J. Colon, S. Das, S. Seal, J. Turkson, J. Zhao, and C.H. Baker, *Sensitization of pancreatic cancer cells to radiation by cerium oxide nanoparticle-induced ROS production*. *Nanomedicine: Nanotechnology, Biology and Medicine*, 2012.
 70. Zhou, X., L.L. Wong, A.S. Karakoti, S. Seal, and J.F. McGinnis, *Nanoceria inhibit the development and promote the regression of pathologic retinal neovascularization in the Vldlr knockout mouse*. *PLoS One*, 2011. **6**(2): p. e16733.
 71. Kong, L., X. Cai, X. Zhou, L.L. Wong, A.S. Karakoti, S. Seal, and J.F. McGinnis, *Nanoceria extend photoreceptor cell lifespan in *tubby* mice by modulation of apoptosis/survival signaling pathways*. *Neurobiology of disease*, 2011. **42**(3): p. 514-523.
 72. Pourkhalili, N., A. Hosseini, A. Nili-Ahmadabadi, S. Hassani, M. Pakzad, M. Baeri, A. Mohammadirad, and M. Abdollahi, *Biochemical and cellular evidence of the benefit of a combination of cerium oxide nanoparticles and selenium to diabetic rats*. *World journal of diabetes*, 2011. **2**(11): p. 204.
 73. Pourkhalili, N., A. Hosseini, A. Nili-Ahmadabadi, M. Rahimifard, M. Navaei-Nigjeh, S. Hassani, M. Baeri, and M. Abdollahi, *Improvement of isolated rat pancreatic islets function by combination of cerium oxide nanoparticles/sodium selenite through reduction of oxidative stress*. *Toxicology mechanisms and methods*, 2012. **22**(6): p. 476-482.
 74. Park, E.-J., J. Choi, Y.-K. Park, and K. Park, *Oxidative stress induced by cerium oxide nanoparticles in cultured BEAS-2B cells*. *Toxicology*, 2008. **245**(1): p. 90-100.
 75. Hirst, S.M., A.S. Karakoti, R.D. Tyler, N. Sriranganathan, S. Seal, and C.M. Reilly, *Anti-inflammatory Properties of Cerium Oxide Nanoparticles*. *Small*, 2009. **5**(24): p. 2848-2856.
 76. Singh, S., A. Kumar, A. Karakoti, S. Seal, and W.T. Self, *Unveiling the mechanism of uptake and sub-cellular distribution of cerium oxide nanoparticles*. *Molecular BioSystems*, 2010. **6**(10): p. 1813-1820.
 77. Mettler Jr, F.A. and G.L. Voelz, *Major radiation exposure—what to expect and how to respond*. *New England Journal of Medicine*, 2002. **346**(20): p. 1554-1561.
 78. Simonsen, L.C., J.W. Wilson, M.H. Kim, and F.A. Cucinotta, *Radiation exposure for human Mars exploration*. *Health physics*, 2000. **79**(5): p. 515-525.
 79. Korst, A., C. Eeltink, J. Vermorken, and W. Van der Vijgh, *Pharmacokinetics of amifostine and its metabolites in patients*. *European Journal of Cancer*, 1997. **33**(9): p. 1425-1429.
 80. Norton, G., *New developments in design and applications for Pelletron accelerators*. *Pramana*, 2002. **59**(5): p. 745-751.

81. Middleton, R., *A versatile high intensity negative ion source*. Nuclear Instruments and Methods in Physics Research, 1983. **214**(2): p. 139-150.
82. Middleton, R., *A versatile high intensity negative ion source*. Nuclear Instruments and Methods in Physics Research, 1984. **220**(1): p. 105-106.
83. Middleton, R., *A negative ion cookbook*. University of Pennsylvania, 1989.
84. Heddle, D.W., *Electrostatic lens systems 2000*: CRC Press.
85. Davis, T. *Charging System*. 2001; Available from: <http://www.pelletron.com/charging.htm>.
86. Ferry, J.A., *Recent developments in electrostatic accelerator technology at NEC*. Nuclear Instruments and Methods in Physics Research Section A: Accelerators, Spectrometers, Detectors and Associated Equipment, 1993. **328**(1): p. 28-33.
87. *How big is a human cell?* [cited 2015 February 2]; Available from: <http://www.weizmann.ac.il/plants/Milo/images/humanCellSize120116Clean.pdf>.
88. BETTEGA P. CALZOLARI SM DOGLIA B. DULIO L. TALLONE AM VILLA, D., *Technical Report: Cell thickness measurements by confocal fluorescence microscopy on C3H10T1/2 and V79 cells*. International journal of radiation biology, 1998. **74**(3): p. 397-403.
89. BELLI F. CERA R. CHERUBINI M. DALLA VECCHIA AMI HAQUE F. IANZINI G. MOSCHINI O. SAPORA G. SIMONE MA TABOCCHINI P. TIVERON, M., *RBE-LET relationships for cell inactivation and mutation induced by low energy protons in V79 cells: further results at the LNL facility*. International journal of radiation biology, 1998. **74**(4): p. 501-509.
90. Belli, M., F. Cera, R.a. Cherubini, A. Haque, F. Ianzini, G. Moschini, O. Sapora, G. Simone, M. Tabocchini, and P. Tiveron, *Inactivation and mutation induction in V79 cells by low energy protons: Re-evaluation of the results at the LNL facility*. International journal of radiation biology, 1993. **63**(3): p. 331-337.
91. Belli, M., R. Cherubini, S. Finotto, G. Moschini, O. Sapora, G. Simone, and M. Tabocchini, *RBE-LET relationship for the survival of V79 cells irradiated with low energy protons*. International journal of radiation biology, 1989. **55**(1): p. 93-104.
92. Incorporated, E., *XCAP Software*, 2015.
93. Stampfer, M.R. and J.C. Bartley, *Human mammary epithelial cells in culture: differentiation and transformation*, in *Breast Cancer: cellular and molecular biology* 1988, Springer. p. 1-24.
94. Stampfer, M.R., *Cholera toxin stimulation of human mammary epithelial cells in culture*. In vitro, 1982. **18**(6): p. 531-537.
95. Seal, S.S., D [private communication], B. Swartz, Editor 2015.
96. Vujaskovic, Z., I.L. Jackson, S. Seal, and S. Das, *Methods of using cerium oxide nanoparticles to mitigate or protect against radiation injury*, 2013, Google Patents.
97. Patil, S., S. Kuiry, S. Seal, and R. Vanfleet, *Synthesis of nanocrystalline ceria particles for high temperature oxidation resistant coating*. Journal of Nanoparticle Research, 2002. **4**(5): p. 433-438.
98. Tsunekawa, S., R. Sivamohan, S. Ito, A. Kasuya, and T. Fukuda, *Structural study on monosize CeO_{2-x} nano-particles*. Nanostructured materials, 1999. **11**(1): p. 141-147.
99. van Meerloo, J., G.J. Kaspers, and J. Cloos, *Cell sensitivity assays: the MTT assay*, in *Cancer Cell Culture* 2011, Springer. p. 237-245.

100. Heatwole, V.M., *TUNEL assay for apoptotic cells*, in *Immunocytochemical Methods and Protocols* 1999, Springer. p. 141-148.
101. *Manual of Click-iT TUNEL Alexa Fluor Imaging assay*. Available from: <http://probes.invitrogen.com/media/pis/mp10245.pdf>.
102. Anandkumar, M., C. Ramamurthy, C. Thirunavukkarasu, and K.S. Babu, *Influence of age on the free-radical scavenging ability of CeO₂ and Au/CeO₂ nanoparticles*. *Journal of Materials Science*: p. 1-10.
103. Folkard, M., *Inactivation of V79 cells by low-energy protons, deuterons and helium-3 ions*. *International journal of radiation biology*, 1996. **69**(6): p. 729-738.
104. Folkard, M., K. Prise, B. Vojnovic, S. Davies, M. Roper, and B. Michael, *The Irradiation of V79 Mammalian Cells by Protons with Energies below 2 MeV: Part I: Experimental Arrangement and Measurements of Cell Survival*. *International journal of radiation biology*, 1989. **56**(3): p. 221-237.
105. Buch, K., T. Peters, T. Nawroth, M. Sanger, H. Schmidberger, and P. Langguth, *Determination of cell survival after irradiation via clonogenic assay versus multiple MTT assay-a comparative study*. *Radiation oncology*, 2012. **7**(1): p. 1-6.
106. Sinclair, W., *CELL CYCLE DEPENDENCE ON THE LETHAL RADIATION RESPONSE IN MAMMALIAN CELLS*, 1972, Argonne National Lab., Ill.
107. Schettino, G., M. Folkard, K. Prise, B. Vojnovic, A. Bowey, and B. Michael, *Low-dose hypersensitivity in Chinese hamster V79 cells targeted with counted protons using a charged-particle microbeam*. 2009.
108. Sugiyama, M., X.-W. Wang, and M. Costa, *Comparison of DNA lesions and cytotoxicity induced by calcium chromate in human, mouse, and hamster cell lines*. *Cancer research*, 1986. **46**(9): p. 4547-4551.
109. Sutherland, J.C., *Repair-dependent cell radiation survival and transformation: an integrated theory*. *Physics in medicine and biology*, 2014. **59**(17): p. 5073.
110. Sontag, W., *A discrete cell survival model including repair after high dose-rate of ionizing radiation*. *International journal of radiation biology*, 1997. **71**(2): p. 129-144.
111. Van Erp, P., J. Boezeman, and P. Brons, *Cell cycle kinetics in normal human skin by in vivo administration of iododeoxyuridine and application of a differentiation marker-- implications for cell cycle kinetics in psoriatic skin*. *Analytical cellular pathology: the journal of the European Society for Analytical Cellular Pathology*, 1996. **11**(1): p. 43-54.
112. Rew, D. and G. Wilson, *Cell production rates in human tissues and tumours and their significance. Part II: clinical data*. *European Journal of Surgical Oncology (EJSO)*, 2000. **26**(4): p. 405-417.
113. Vynckier, S., D. Bonnett, and D. Jones, *Code of practice for clinical proton dosimetry*. *Radiotherapy and oncology*, 1991. **20**(1): p. 53-63.
114. Thieberger, P., H. Abendroth, J. Alessi, L. Cannizzo, C. Carlson, A. Gustavsson, M. Minty, and L. Snydstrup, *A very thin Havar film vacuum window for heavy ions to perform radiobiology studies at the BNL Tandem*, 2011, Brookhaven National Laboratory (BNL) Tandem Van De Graaff.
115. Deshpande, S., S. Patil, S.V. Kuchibhatla, and S. Seal, *Size dependency variation in lattice parameter and valency states in nanocrystalline cerium oxide*. *Applied Physics Letters*, 2005. **87**(13): p. 133113-133113-3.

116. Korsvik, C., S. Patil, S. Seal, and W.T. Self, *Superoxide dismutase mimetic properties exhibited by vacancy engineered ceria nanoparticles*. Chem. Commun., 2007(10): p. 1056-1058.
117. Juzenas, P., W. Chen, Y.-P. Sun, M.A.N. Coelho, R. Generalov, N. Generalova, and I.L. Christensen, *Quantum dots and nanoparticles for photodynamic and radiation therapies of cancer*. Advanced drug delivery reviews, 2008. **60**(15): p. 1600-1614.
118. Chithrani, D.B., S. Jelveh, F. Jalali, M. van Prooijen, C. Allen, R.G. Bristow, R.P. Hill, and D.A. Jaffray, *Gold nanoparticles as radiation sensitizers in cancer therapy*. Radiation Research, 2010. **173**(6): p. 719-728.
119. Maier-Hauff, K., F. Ulrich, D. Nestler, H. Niehoff, P. Wust, B. Thiesen, H. Orawa, V. Budach, and A. Jordan, *Efficacy and safety of intratumoral thermotherapy using magnetic iron-oxide nanoparticles combined with external beam radiotherapy on patients with recurrent glioblastoma multiforme*. Journal of neuro-oncology, 2011. **103**(2): p. 317-324.
120. Le Duc, G.r., I. Miladi, C. Alric, P. Mowat, E. Bräuer-Krisch, A. Bouchet, E. Khalil, C. Billotey, M. Janier, and F.o. Lux, *Toward an image-guided microbeam radiation therapy using gadolinium-based nanoparticles*. ACS nano, 2011. **5**(12): p. 9566-9574.
121. Porcel, E., S. Liehn, H. Remita, N. Usami, K. Kobayashi, Y. Furusawa, C. Le Sech, and S. Lacombe, *Platinum nanoparticles: a promising material for future cancer therapy?* Nanotechnology, 2010. **21**(8): p. 085103.
122. Chattopadhyay, S., S.K. Dash, S. Tripathy, B. Das, S. Kar Mahapatra, P. Pramanik, and S. Roy, *Cobalt oxide nanoparticles induced oxidative stress linked to activation of TNF- α /caspase-8/p38-MAPK signaling in human leukemia cells*. Journal of Applied Toxicology, 2015.

